REVIEW

Progress in Electrolyte Engineering of Aqueous Batteries in a Wide Temperature Range

Lingjun He[1,3] · Chuyuan Lin[1] · Peixun Xiong[2] · Hui Lin[1] · Wenbin Lai[1] · Jingran Zhang[1] · Fuyu Xiao[1] · Liren Xiao[1,3] · Qingrong Qian[1,4] · Qinghua Chen[1,4] · Lingxing Zeng[1,4]

Abstract

Aqueous rechargeable batteries are safe and environmentally friendly and can be made at a low cost; as such, they are attracting attention in the field of energy storage. However, the temperature sensitivity of aqueous batteries hinders their practical application. The solvent water freezes at low temperatures, and there is a reduction in ionic conductivity, whereas it evaporates rapidly at high temperatures, which causes increased side reactions. This review discusses recent progress in improving the performance of aqueous batteries, mainly with respect to electrolyte engineering and the associated strategies employed to achieve such improvements over a wide temperature domain. The review focuses on five electrolyte engineering (aqueous high-concentration electrolytes, organic electrolytes, quasi-solid/solid electrolytes, hybrid electrolytes, and eutectic electrolytes) and investigates the mechanisms involved in reducing the solidification point and boiling point of the electrolyte and enhancing the extreme-temperature electrochemical performance. Finally, the prospect of further improving the wide temperature range performance of aqueous rechargeable batteries is presented.

Keywords Aqueous batteries · Electrolyte engineering · Wide temperature range · Hydrogen bond

Lingjun He and Chuyuan Lin have contributed equally to this work.

✉ Peixun Xiong
xiongpeixun@163.com

✉ Fuyu Xiao
Fuyu-Xiao@outlook.com

✉ Lingxing Zeng
zenglingxing@fjnu.edu.cn

1 Engineering Research Center of Polymer Green Recycling of Ministry of Education, Fujian Key Laboratory of Pollution Control and Resource Reuse, College of Environmental and Resources, Fujian Normal University, Fuzhou 350007, China

2 Inorganic Chemistry I, Technische Universität Dresden, Bergstrasse 66, 01069 Dresden, Germany

3 College of Chemistry and Materials Science, Fujian Normal University, Fuzhou 350007, China

4 Key Laboratory of Advanced Energy Materials Chemistry (Ministry of Education), College of Chemistry, Nankai University, Tianjin 300071, China

Introduction

It is becoming increasingly obvious that conventional fossil-fuel-based energy sources are unable to meet global energy requirements due to the escalating global energy demands and environmental challenges. As renewable energy sources (such as wind, solar, and tidal power) are intermittent in nature, electrochemical energy storage devices will need to play a vital role in supplying consistent energy [1, 2]. Presently, lithium-ion batteries (LIBs) dominate the field and are the most extensively employed electrochemical energy storage systems [3–6]. However, LIBs are extremely expensive to produce, and Li resources are finite. In addition, the use of organic electrolytes (predominantly ethylene carbonate) in commercially available LIBs is associated with significant flammability risks and safety concerns [7–10], and organic electrolyte batteries also require stringent environmental processing. Furthermore, the burgeoning demand for flexible and wearable electronics renders organic electrolyte batteries less than ideal, as they deform under typical usage conditions [11–13].

Compared to organic-based LIBs, aqueous rechargeable batteries (ARBs) (comprising Li ion, sodium ion, potassium

ion, and zinc ion) are considered to be safe, economical, and environmentally promising alternatives. The use of water as an electrolyte solvent in ARBs provides the following advantages: (1) intrinsic safety because water is inflammable, (2) a cheap aqueous solvent, (3) batteries that are easy to assemble and no strict manufacturing environment is required, (4) an aqueous electrolyte with high ionic conductivity that is approximately two orders of magnitude higher than that of organic electrolytes, and (5) an aqueous solvent that is nontoxic and does not pollute the environment [14–16]. These advantages collectively make ARBs a promising substitute for use in specific application scenarios, such as grid-scale energy storage, and in portable, flexible, wearable electronic devices [17–20].

To use of ARBs is promising in a wide range of applications and unique applications (such as polar, space, deep-sea and high-altitude exploration). Although it is expected that they can be adapted to different temperature environments, the aqueous electrolyte exhibits extreme-temperature sensitivity [21, 22]. In this respect, the high freezing point of the aqueous electrolyte is a fatal problem when operating in high-latitude cold regions. The probability of forming hydrogen bonds (HBs) becomes progressively higher than the likelihood of breaking bonds at temperatures lower than 4 °C, which leads to an increase in viscosity, and solidification can occur as the temperature lowers further. In addition, the phase transitions of the solvent water alter the physicochemical properties of the bulk electrolyte. Although the freezing point of the aqueous electrolyte is lowered by the addition of solutes according to Raoult's law [23], the viscosity of the electrolyte gradually increases as the temperature drops and the electrolyte concentration rises [24–26]. Even more detrimental is the combined effect of the high viscosity and the dielectric effect, which reduces the ionic conductivity of the electrolyte (σ) (Eq. (1)) [27–29],

$$\sigma = \sum_i n_i \mu_i z_i e \tag{1}$$

where n_i is the free ion number; μ_i is the ionic mobility; and z_i is the valence order of ions. This increases the ohmic resistance of the electrolyte and concentration polarization at the electrolyte/electrode interface, thereby causing battery failure during correct operation at low temperatures [30]. In addition, electrolyte freezing hinders the wettability of the electrode–electrolyte interface, and this also seriously affects the low-temperature performance of the ARB [31, 32]. Although increasing the solute concentration appropriately increases the boiling point (T_b) of aqueous electrolytes (Eq. (2)),

$$\Delta T_b = T_b - T_b^* = K_b \times m \tag{2}$$

where ΔT_b is the boiling point variation; T_b^* is the boiling point of pure water (101.325 kPa); K_b is the boiling point decrease constant of the solvent; and m is the concentration of ions (mol/kg); the high volatility of water and the instability of the electrolyte/electrode interface at high temperatures still limit the use of ARBs in high-temperature environments [33, 34].

All these limitations are major challenges hindering the further development of ARBs. Therefore, to promote the development of high-performance electrochemical energy storage devices and to meet the requirements of real applications in various fields, it is important to develop efficient modification strategies that extend the temperature range of ARBs, and it is necessary to investigate the mechanism of action and constitutive relationships involved [35, 36].

As it is paramount to select a suitable electrolyte to give ARBs a wide temperature range performance, and it is crucial to urgently address the temperature problem of ARBs, this review systematically summarizes recent research progress made in electrolyte engineering over a wide temperature range (Fig. 1). The large amount of research based on electrolyte research demonstrates that the physical and chemical properties of the electrolyte are key factors in the mass transport, energy storage mechanism, reaction kinetics, and side reactions of ARBs at extreme temperatures. In this respect, we first discuss the strategies associated with the use of high-concentration electrolytes, electrolyte additives, and hydrogel electrolytes in lowering the freezing point of the electrolyte and improving the low-temperature
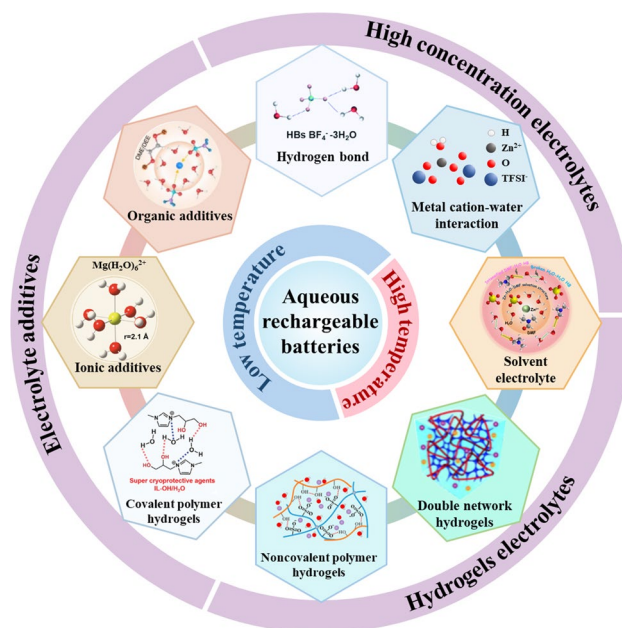

Fig. 1 Electrolyte strategy for rechargeable batteries in water systems over a wide temperature range

performance of ARBs. We then show that the high temperature performance of ARBs can be improved by adding highly thermally stable substances into the electrolyte or by reducing the water content of the electrolyte. Finally, this review provides certain perspectives for the rational design and mechanistic investigation of electrolytes over a wide temperature range and an outlook on the future development of ARBs across a wide temperature range.

Aqueous Rechargeable Battery (ARB) at Low Temperature

In low-temperature conditions, the water-based electrolyte can constrain the ARB performance. Despite the previously mentioned notable advantages of ARBs, freezing of water at low temperatures poses practical limitations. This freezing phenomenon leads to diminished ionic conductivity, inadequate de-solvation, heightened interfacial impedance, and sluggish ion transport, which significantly impedes the functionality of aqueous batteries in low-temperature environments. The primary approach to enhancing the low-temperature performance of batteries involves improving the electrolyte's ionic conductivity and enhancing the diffusion coefficient of ions within the electrode material under these conditions. Therefore, research efforts have been focused on lowering the freezing point of the electrolyte and augmenting its ionic conductivity. The freezing process of water is regarded as a phase transition from disordered water to ordered ice, driven by the formation of HBs; therefore, by inhibiting the formation of HBs between water molecules, it is possible to reduce the freezing point. Electrolyte modification has emerged as an effective strategy for enhancing the low-temperature performance of ARBs. In this section, we investigate how electrolyte strategies can effectively address the limitations of current ARBs in low-temperature scenarios.

Aqueous High-Concentration Electrolytes

The behavior of water molecules changes when the temperature decreases below 0 °C, which causes the formation of an additional 0.52 HBs; this leads to the reorganization of water molecules from a disordered state to an ordered one and results in the formation of solid ice [37, 38]. By weakening the HBs between water molecules, it is possible to effectively reduce the freezing point of aqueous electrolytes. In this respect, Raoult's law states that for dilute solutions of non-electrolytes with high boiling points, the decrease in the freezing point (ΔT_f) is directly proportional to the molar concentration of the solution [31, 32], and this can be expressed as

$$\Delta T_f = T_{water} - T_{solution} = K_{f \cdot m}$$

where ΔT_f represents the freezing point depression; T_{water} is the thermodynamic freezing point of the solvent (which is 0 °C for water); K_f is the freezing point depression constant measured in units of K·kg/mol or °C·kg/mol (with a value of 1.86 °C kg/mol for water); and the subscript m denotes the molar concentration of the solution. It is important to note that the value of K_f is solely dependent on the solvent and remains unaffected by the solute. As an illustration, a solution of $ZnCl_2$ at a concentration of 1 mol/kg has a freezing point of −5.58 °C. Although this equation is applicable to dilute solutions, literature reports have indicated that increasing the solute concentration to form high-concentration electrolytes is an effective approach used to reduce the freezing point of electrolytes [39].

The development of "water-in-salt" electrolytes (WiSE) has provided new possibilities for the development of high-energy ARBs, as these resemble ionic liquids and have high salt and low water concentrations [40, 41]. By utilizing electrolytes with elevated salt concentrations, the electrochemical stability window is expanded, which enhances the surface structure of the electrode materials within the aqueous environment [42]. Figure 2 shows the effect of high concentrations of ions with different charges on the HB network between water molecules. The interactions between free cations, anions, and aqueous solvents in highly concentrated electrolytes directly determine the effectiveness of lowering the freezing point of aqueous electrolytes (Fig. 2a) [43]. For instance, the strong dipole–dipole forces between Zn^{2+} and O in the high-concentration electrolytes cause rearrangement of the coordination structure of H_2O, and as Zn^{2+} binding is preferential to the formation of intermolecular HBs [36], the freezing point is significantly reduced.

Through theoretical calculations, Zhang et al. [23] found that Zn^{2+}–H_2O possessed a higher binding energy of −98.5 kcal/mol compared to that of H_2O–H_2O (Fig. 2b). Building on this insight, a high concentration of $ZnCl_2$ (7.5 mol/L) was employed as the electrolyte in a Zn‖polyaniline (PANI) cell. The abundance of Zn^{2+} in the electrolyte broke the HBs between water molecules, allowing the cell to operate at an ultimate temperature of −90 °C, with a stable cycling performance at −70 °C (84.9 mAh/g, ~2000 cycles), and this battery could operate at the lowest to highest recorded Earth's surface temperatures from −89.2 °C (Death Valley, California, USA, 1913) to 56.7 °C (Vostok Station, Antarctica, 1983). Very few cells are capable of operating at this temperature range (Fig. 2c), although a similar phenomenon is achieved with the potassium-based WiSE electrolyte.

Through Raman spectroscopy analysis, Liang et al. [44] showed that a large amount of free molecular water exists in a low concentration in a 1 mol/L KOTF electrolyte, while
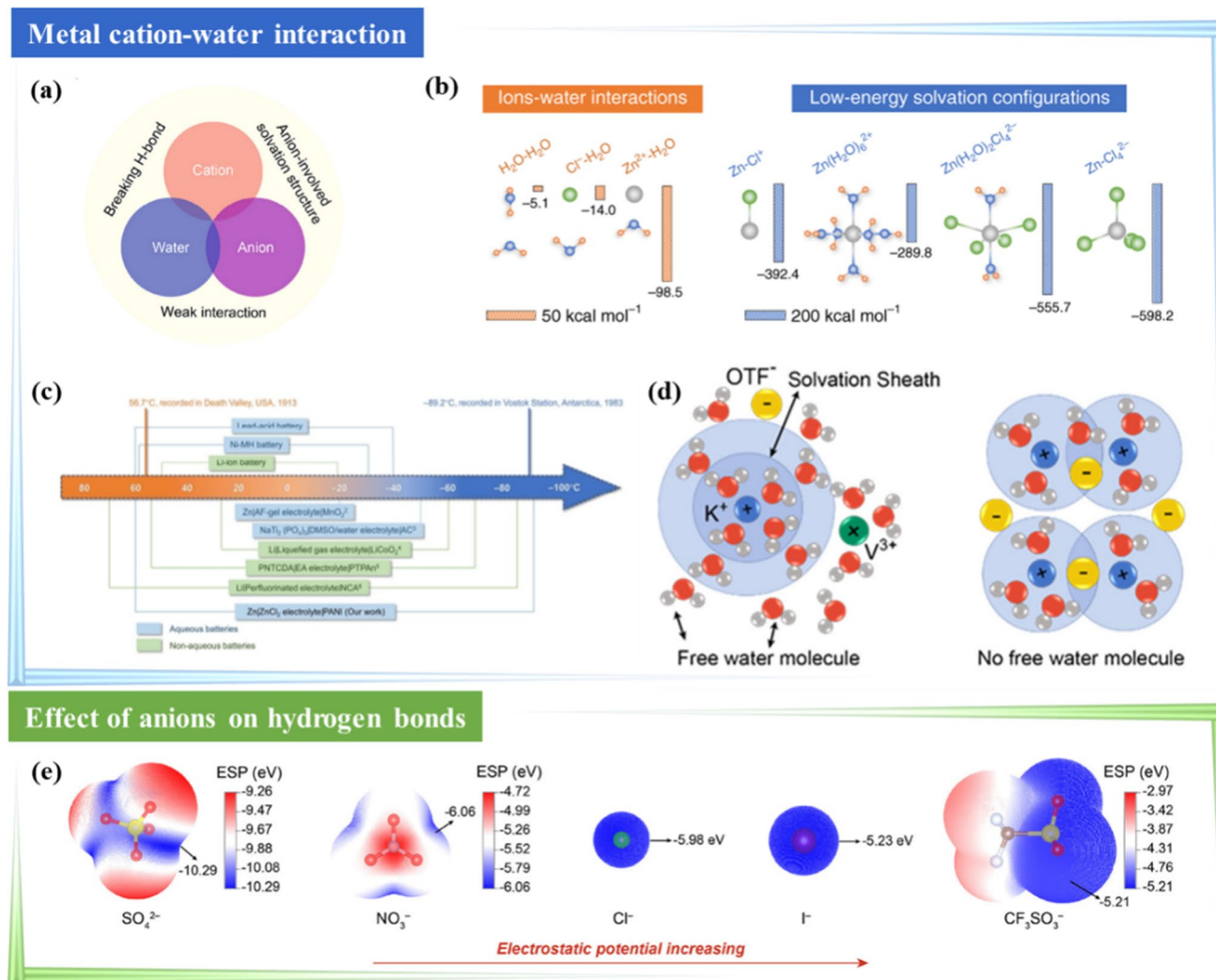
Fig. 2 a Schematic illustration of mutual interactions between cations, anions, and water solvent. **b** Calculated interactions between ions and water and the formation energies of Zn^{2+} solvation configurations. **c** Operating temperature window of existing batteries. **b** and **c** were reproduced with permission from Ref. [24]. Copyright © 2020 Springer Nature. **d** Schematic illustration of the solvation structure of low-concentration 1 mol/L KOTF and high-concentration 22 mol/L KOTF electrolytes. Reproduced with permission from Ref. [44]. Copyright © 2021 American Chemical Society. **e** Negative ESP mapping of anions SO_4^{2-}, NO_3^-, Cl^-, I^-, and $CF_3SO_3^-$. **a** and **e** were reproduced with permission from Ref. [43]. Copyright © 2021 American Chemical Society

the weak HBs of a 22 mol/L KOTF remain unchanged, and the proportion of strong HBs is substantially reduced. These observed phenomena are attributed to the strong solvation effect of K^+ ions (Fig. 2d), which effectively restricts the movement of H_2O molecules within the solvation sheath of K^+ [45, 46]. As a result, the freezing point of this electrolyte is significantly lowered to -39 °C, and this antifreeze property gives the battery good stability, even at ultra-low temperatures of -30 °C.

As mentioned above, multivalent cations can lower the freezing point of aqueous electrolytes, but anions can also significantly improve the low-temperature electrochemical properties of ARBs. Different anions in the Hofmeister sequence have been reported to have different effects on

HBs. Chaotropic anions, such as I^-, can reduce the density and strength of the HBs between water molecules; in contrast, kosmotropic anions, such as SO_4^{2-}, increase the number of HBs and their strength. Zhang's group [43] summarized the magnitude of the electrostatic potential (ESP) values of different anions using theoretical calculations and spectroscopic analysis techniques, and they explained the effect of anions with different ESP values on the solvation structure, HB number, and the HB strength of Zn^{2+} (Fig. 2e). The results showed that $CF_3SO_3^-$ had the highest ESP value and the lowest binding energy to the H_2O/cation compared to the other ions, which indicated that this anion had the weakest interaction with Zn^{2+} and therefore the highest Zn–water coordination number in the $Zn(CF_3SO_3)_2$ electrolyte. As a

consequence, there were fewer HBs between the free water molecules, and the Fourier transform infrared spectroscopy (FTIR) results further confirmed that the lower HB strength corresponded to a lower thermodynamic freezing point. The electrochemical performance test results showed that the Zn∥2 mol/L Zn(CF₃SO₃)₂∥V₂O₅ cell retained functionality at −30 °C with a capacity of 194.1 mA h/g when the current density was 1 A/g, and it showed a capacity retention rate of 81.7% after 1000 cycles, compared to the rest of the low-temperature aqueous cells, which at the appropriate low-temperature conditions with higher capacity and cycling stability.

Although increasing the concentration of an electrolyte can effectively lower its freezing point, a higher concentration can be detrimental to its functionality. Indeed, when the concentration of salt in the electrolyte exceeds a certain threshold, salt crystallization becomes a concern. The solubility of electrolyte salts typically increases with temperature, meaning that lower temperatures lead to lower solubility. Different salts have distinct physical properties, and the combination of their concentrations and temperatures determines the specific crystallization zones for each salt. Therefore, the concentration of the aqueous electrolytes needs to be properly balanced to achieve optimum results at low temperatures. Becker and co-workers [47] discovered that the use of asymmetric anions in high-concentration electrolytes effectively inhibited the crystallization of highly concentrated electrolytes at low temperatures. Building on this finding, they proposed a mixed electrolyte consisting of asymmetric LiPTFSI (lithium bis(trifluoromethanesulfonyl) imide) and LiOTf (lithium trifluoromethanesulfonate). LiPTFSI exhibits exceptional solubility at room temperature, with a solubility exceeding 30 mol/L, and the addition of a second anion, LiOTf, to the electrolyte mixture resulted in an increase in the mixing entropy. Compared with 21 mol/L LiTFSI and 20 mol/L LiOTf, this increase in entropy of the mixed electrolyte (nLiTFSI/LiOTf = 15 mol/L/5 mol/L) resulted in a reduction in the liquid phase line temperature, further reducing the freezing point from ∼ 20 to −14 °C (Fig. 3a).

Reber et al. [48] adopted the same strategy when using an asymmetric NaFSI/NaFTFSI electrolyte. As shown in Fig. 3b, the 25 mol/L NaFSI + 10 mol/L NaFTFSI electrolyte did not crystallize during the cooling scan and remained liquid at room temperature after six months. In addition, the asymmetric anion inhibited the formation of the long-range order and thus effectively suppressed crystallization. The NaFTFSI additive containing asymmetric anions not only inhibited the crystallization of the highly concentrated electrolyte but also lowered its freezing point. Furthermore, the NTP/NVPOF full cell with the mixed anionic electrolyte reached a total of 500 cycles at −10 °C, maintaining a high cycle stability (Fig. 3c).

By incorporating such asymmetric anions into the electrolyte, the researchers aimed to enhance the low-temperature performance of the electrolyte and prevent salt crystallization issues arising at high concentrations. The use of highly concentrated electrolytes is logical in ARBs, as the electrochemical stability window of water can be extended, and operation can occur over a wider temperature range, which is beneficial for various battery applications.

An alternative approach is to introduce elements containing hydrogen-bonded receptors, which compete with the HBs between water molecules, resulting in a reduction in the freezing point of water. For example, Sun et al. [49] applied a 4 mol/L Zn(BF₄)₂ electrolyte in low-temperature aqueous zinc-ion batteries (AZIBs) and achieved an extraordinarily low freezing point of −122 °C while maintaining a high ionic conductivity of 1.47 mS/cm at −70 °C, and this was applied to high-performance AZIBs. Comprehensive spectral analyses and molecular dynamics (MD) simulations have shown that BF_4^- contains four extremely electronegative F atoms, which easily form O–H···F bonds with H₂O and can efficiently break the original H-bonding network between the H₂O molecules to give the electrolyte an ultra-low freezing point (Fig. 3d–f). The 4 mol/L Zn(BF₄)₂-based electrolyte enabled the Zn∥Tetrachlorobenzoquinone (TCBQ) cell to exhibit an excellent electrochemical performance over a wide temperature range of −95 to 25 °C, with a capacity of up to 63.5 mAh/g and an energy density of 76.2 Wh/kg at −95 °C (Fig. 3g).

The concentrated electrolyte strategy is attracting considerable attention due to its several advantages, as follows: it (1) lowers the freezing point of the electrolyte [50], (2) extends the electrochemical stability window of the electrolyte [51, 52], (3) reduces the cathode dissolution and anode corrosion [53], (4) accelerates the electrode reactions, and (5) increases the metal ion migration number. These advantages provide ARBs with excellent low-temperature electrochemical performance. However, the disadvantages of highly concentrated electrolytes cannot be ignored, and these include low conductivity, high viscosity due to the strong cation–anion-ion coupling, salt precipitation when the temperature drops, and the high associated costs; therefore, continuous research is required to overcome these issues [54–56].

Hydrogel Electrolyte

In addition to tuning the concentration of the electrolyte, the development of hydrogels (cross-linked networks of hydrophilic polymer chains dispersed in water) has helped to alleviate the problem of electrode dissolution and to mitigate the electrochemical performance deteriorating at a temperature below 0 °C. Due to the development of a hydrogel that maintains good flexibility at sub-zero temperatures, flexible
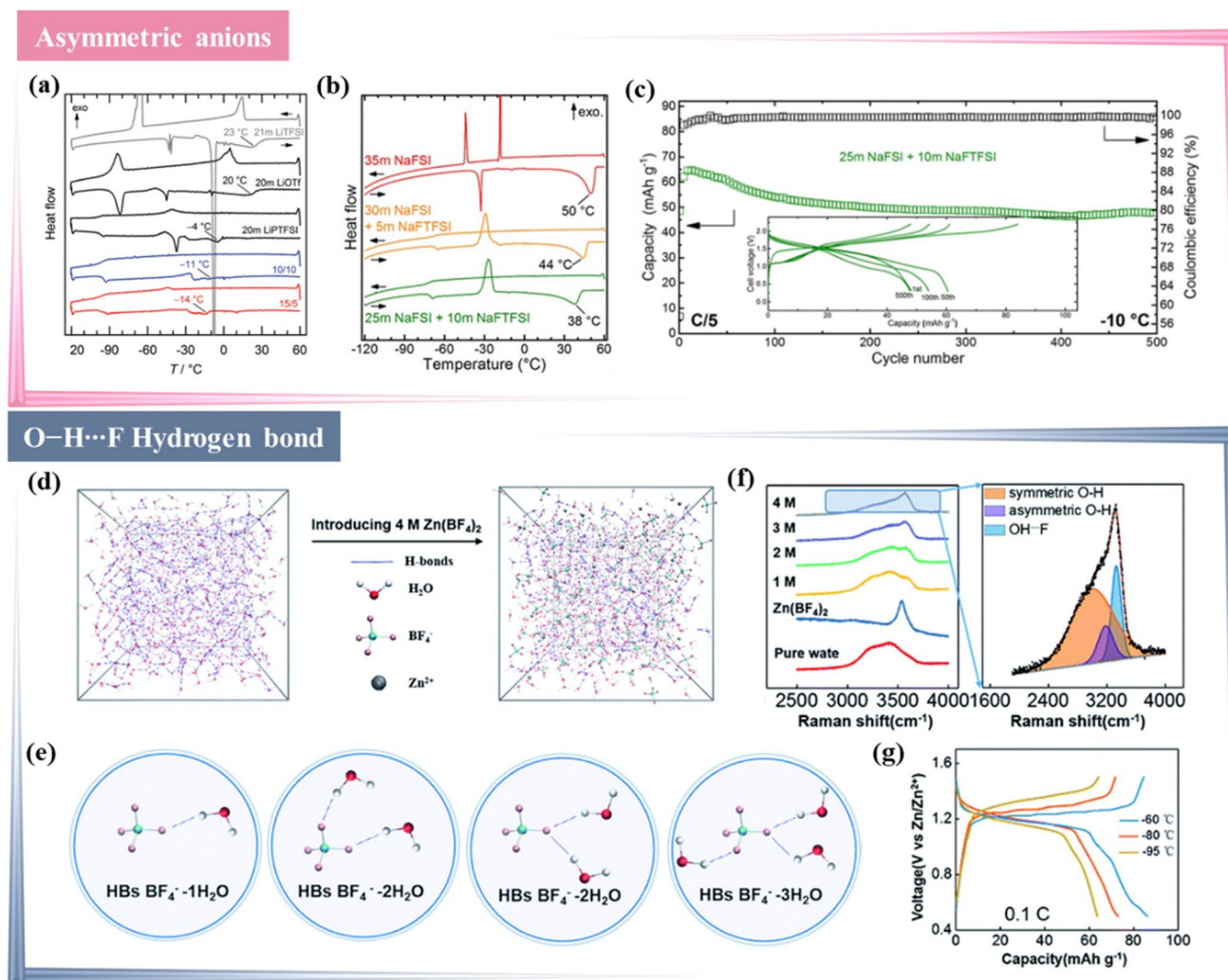
Fig. 3 a Differential scanning calorimetry (DSC) curves of different ~20 mol/L electrolytes recorded at a scan rate of 1 K/min from 60 to 120 °C and back to 60 °C. Reproduced with permission from Ref. [47]. Copyright © 2019 Royal Society of Chemistry. b DSC curves of 35 mol/L LiFSI and mixed lithium electrolytes containing symmetric FSI and asymmetric FTFSI or symmetric TFSI anions, respectively, during scans from 60 to −120 °C and back to 60 °C. c Cycling data of the −10 °C cell shown in part a for a total of 500 cycles. b and c were reproduced with permission from Ref. [48]. Copyright © 2019 American Chemical Society. d Snapshot of the MD simulation of water and 4 mol/L Zn(BF$_4$)$_2$ electrolyte. The dashed blue line represents the HBs. e Different types of O–H⋯F HBs from the snapshot. f Raman spectra of the O–H bond and the fitted O–H stretching vibration representing the symmetric, asymmetric OH⋯O and OH⋯F HBs. g Galvanostatic charge–discharge curves of Zn‖TCBQ battery at −60 °C. d, e, f, and g were reproduced with permission from Ref. [49]. Copyright © 2021 Royal Society of Chemistry

low-temperature quasi-solid-state batteries can now be fabricated using an anti-freezing hydrogel electrolyte. Hydrogels are commonly regarded as semi-solid electrolytes in which the solid polymer backbone retains a large amount of free water internally through hydrophilic groups [57]. Competing interactions between water molecules and the different surrounding chemical functional groups (i.e., polymers) control the antifreeze properties of hydrogels [58, 59]. Therefore, the type of terminal group of the polymer backbone is a factor determining the antifreeze capacity. The results of density flooding theory calculations (Fig. 4a) show that the interaction energy (Eint) between two water molecules (O–H⋯O) is

−5.75 kcal/mol [60]. The Eint achieved between polyacrylic acid (PAA) and water molecules is almost three times that of O–H⋯O, and this strong van der Waals force can disrupt the HBs between water molecules to increase the barrier to ice crystal formation, which maintains sufficient flexibility and ionic conductivity of the hydrogel electrolyte at low temperatures.

Covalent Polymer Hydrogels

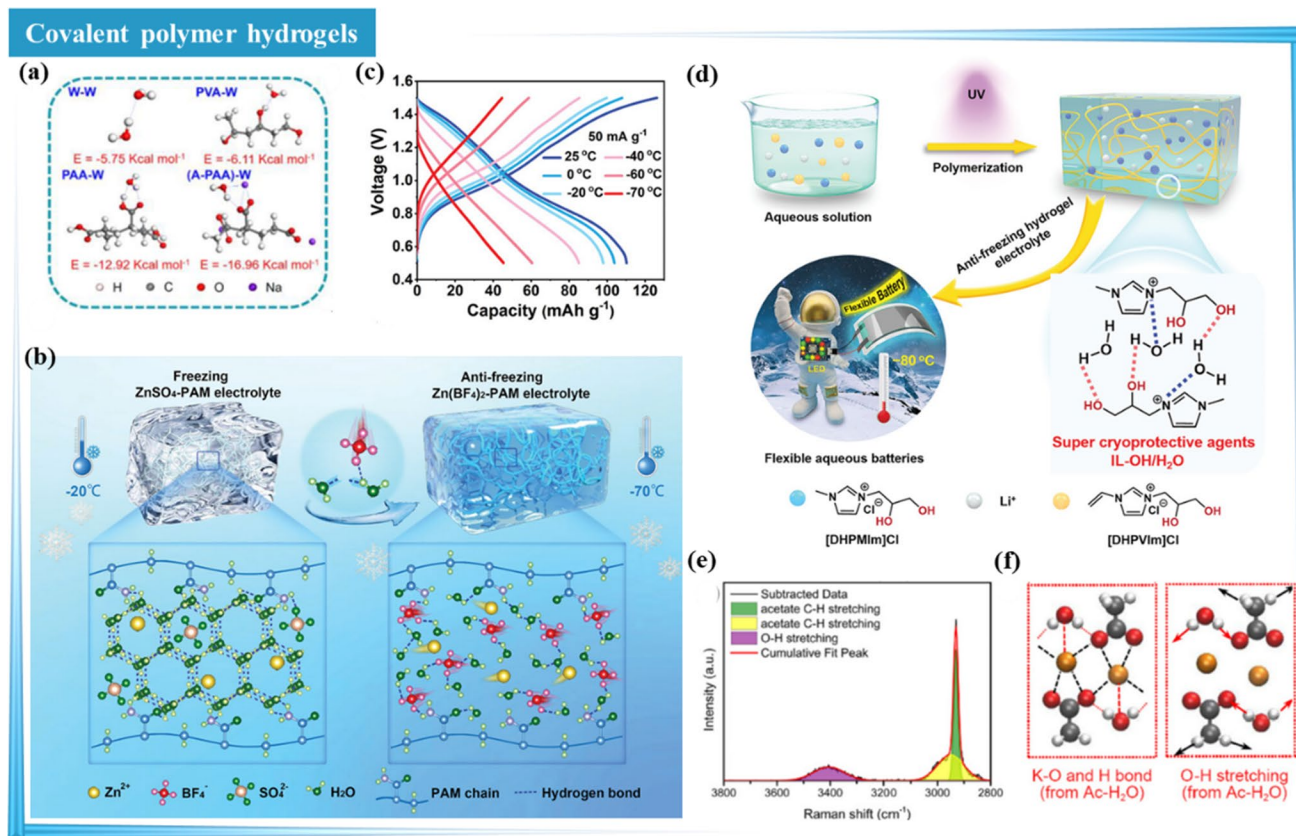Polymer hydrogels are based on covalent cross-linking and are the most commonly employed semi-solid electrolyte

Fig. 4 a Molecular models used to simulate interactions between water molecules and different terminal groups in polymers. Reproduced with permission from Ref. [60]. Copyright © 2020 Wiley. **b** Schematic diagram and mechanism of the anti-freezing hydrogel electrolytes. **c** Galvanostatic charge/discharge curves of $Zn(BF_4)_2$–PAM electrolyte-based flexible zinc-ion batteries at different temperatures. **b** and **c** were reproduced with permission from Ref. [61]. Copyright © 2023 Wiley. **d** Synthesis schematic and mechanisms of the antifreeze PIL-OH-based hydrogel electrolyte. Reproduced with permission from Ref. [62]. Copyright © 2021 Wiley. **e** Raman spectrum of polymer-free CH_3COOK (KAc) gel electrolyte. **f** Density functional theory simulated structures of polymer-free CH_3COOK (KAc) gel electrolyte when the concentration of KAc up to 48 mol/L. **e** and **f** were reproduced with permission from Ref. [63]. Copyright © 2021 Elsevier

type. The introduction of different concentrations of metal salt solutions in the preparation of covalent hydrogels not only improves the ionic conductivity of hydrogel electrolytes but also optimizes their flexibility and solidification points, as shown in Fig. 4. In this respect, Shi et al. [61] synthesized an antifreeze hydrogel electrolyte based on zinc tetrafluoroborate ($Zn(BF_4)_2$) and polyacrylamide (PAM). Due to the strong electronegativity of the F atom, the BF_4^- anion replaced the O–H···O between the free water molecules by forming O–H···F in the $Zn(BF_4)_2$–PAM hydrogel electrolyte, which remained unfrozen even at − 70 °C at low temperatures (Fig. 4b). As a result, the $Zn(BF_4)_2$–PAM electrolyte-based flexible zinc-ion batteries exhibited high adaptation to low temperatures (Fig. 4c). In addition, Hu et al. [62] developed a "two-in-one" cryoprotectant, a hydroxylated functionalized polyionic liquid (PIL-OH)-based hydrogel electrolyte, for use in aqueous LIBs. The synergistic interaction of

ionic hydration and formation of HBs between PIL-OH and water molecules interrupted the water molecule's original hydrogen-bonding network (Fig. 4d) and lowered the freezing point of the water to below − 80 °C. The PIL-OH hydrogel has opened a new avenue in achieving the practical application of wearable and flexible water batteries in ultra-low-temperature environments (e.g., in the Arctic and Antarctic). However, at high salt concentrations, the freezing point decreases depending on the molar concentration of the solution. Liu et al. [63] developed a polymer-free CH_3COOK (KAc) gel electrolyte with an ultra-high salt-to-water molar ratio of 1:1.16 (KAc/H_2O). The Raman spectrum (Fig. 4e) showed that there was no O–H···O, and only the hydrogen band of Ac^- associated with water, which indicated that all water molecules interacted with K^+ and Ac^-, thereby resulting in a high salt concentration gel with a low freezing point (Fig. 4f).

Noncovalent Polymer Hydrogels

The non-covalently cross-linked supramolecular polymer is another type of hydrogel that possesses distinctive self-healing, high toughness, and stretchability. The non-covalent interaction with dynamic reversibility includes interactions with multiple HBs, metal coordination, π–π interactions, and host–guest interactions. Through the modification of solvent and salt solutions, noncovalent hydrogels based on different types of interactions have also been found to exhibit different physical and chemical properties at low temperatures (Fig. 5). Recently, Mo et al.

[64] designed a silk fibroin-based supramolecular hydrogel electrolyte through host–guest interactions between grafted supramolecular β-cyclodextrin and adjacent amino acid molecules on silk fibroin chains and PAA chains (Fig. 5a). Different from the self-healing mechanism through HBs, the host–guest interaction of the supramolecule is independent of temperature; therefore, the freezing point of this hydrogel is lower than that of conventional PAA hydrogel (Fig. 5b). A high salt concentration is usually introduced to modify the hydrogel and further lower the freezing point, increase water retention, and improve the reversibility of metal electrolytes. In this respect, Fu
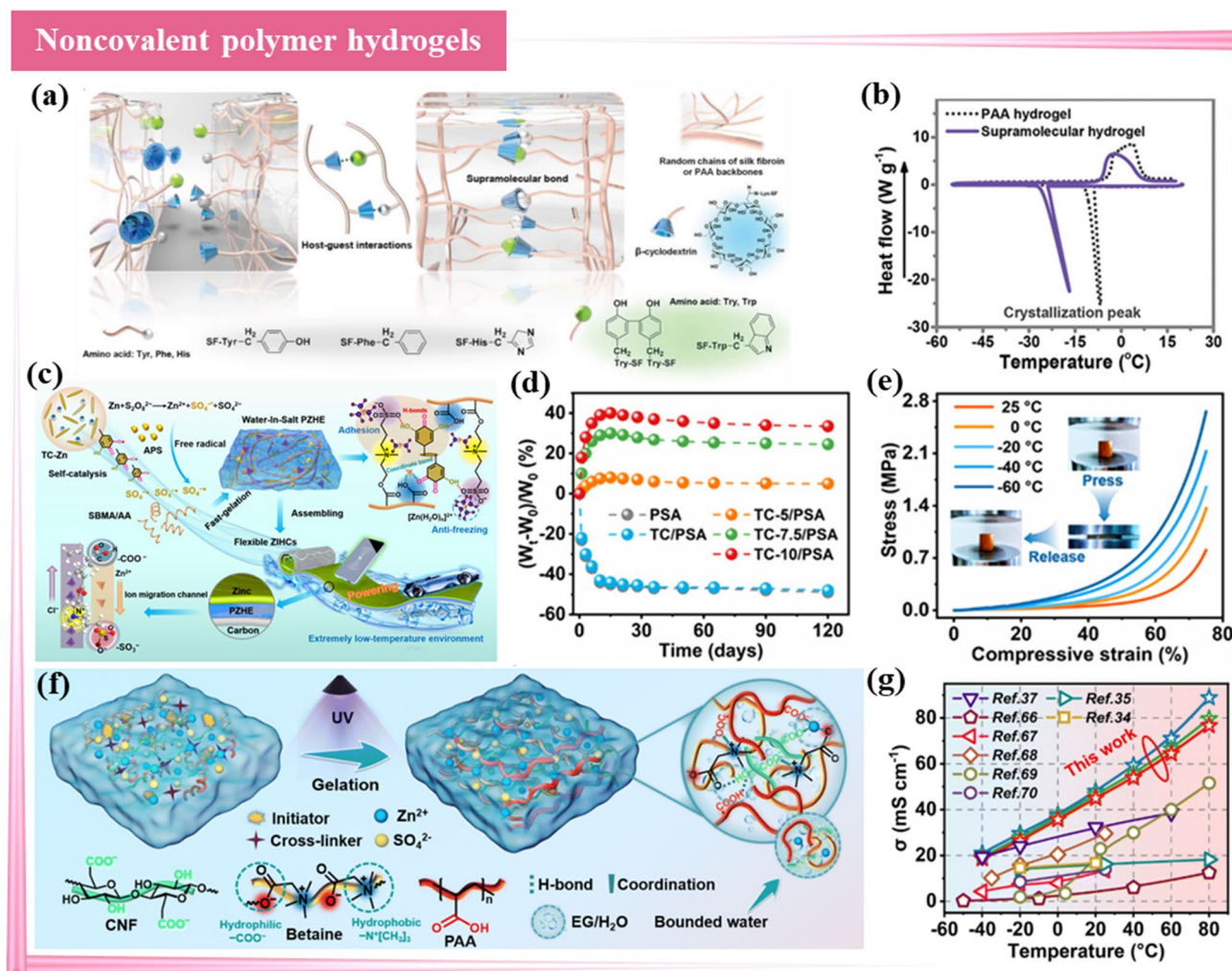

Fig. 5 **a** Engineering and structure of silk fibroin-based supramolecular hydrogel electrolyte through host–guest interactions. **b** DSC curves of silk fibroin-based supramolecular hydrogel electrolyte and PAA hydrogel electrolyte. **a** and **b** were reproduced with permission from Ref. [64]. Copyright © 2021 Wiley. **c** Synthesis schematic of the PZHE by a self-catalytic nano-reinforced strategy. **d** Weight ratio results of PZHE with different ZnCl₂ concentrations. **e** Compressive stress–strain results for the PZHE with 7.5 mol/L ZnCl₂ from −60 to 25 °C, respectively. Inset photographs reveal that the PZHE with 7.5 mol/L $ZnCl_2$ hydrogel electrolytes retained elasticity even when stored for over 1 d at −60. °C **c**, **d**, and **e** were reproduced with permission from Ref. [65]. Copyright © 2021 American Chemical Society. **f** Schematic of supramolecular zwitterion hydrogel electrolytes synthesized by Fu et al. **g** Comparison between the ionic conductivity of this supramolecular zwitterion hydrogel and that of previously reported results. **f** and **g** were reproduced with permission from Ref. [66]. Copyright © 2023 Royal Society of Chemistry

et al. [65] synthesized a polyzwitterionic hydrogel electrolyte (PZHE) using a self-catalytic nano-reinforced strategy and further formed a salt-in-water PZHE with high electrical conductivity and strong interfacial adhesion by filling it with 7.5 mol/L $ZnCl_2$ (Fig. 5c). The colligative property of the concentrated $ZnCl_2$, resulted in a lower water vapor pressure within this salt-in-water PZHE than that in the environment; therefore, the total mass and volume increased slightly after 120 d of storage in an open environment, exhibiting a good water retention capacity (Fig. 5d). It also provided over 420% tensile elasticity and 75% compressive strain at -60 °C, thus accommodating rigorous deformation, including compression, folding, rolling, bending, and twisting (Fig. 5e).

To enhance the ion conductivity of hydrogel electrolytes at low temperatures, Fu et al. [66] synthesized supramolecular zwitterion hydrogel electrolytes by combining supramolecular betaine with nanofiber-reinforced covalently cross-linked PAA in a $ZnSO_4$/ethylene glycol (EG) electrolyte, and this provides outstanding self-healing and anti-freezing capabilities because of the many dynamic coordination bonds and multiple HBs originating from the supramolecular betaine chains, PAA chains, and binding EG in the polymer network (Fig. 5f). In synergy with its special 3D interoperable Zn^{2+} transport channel, which profits from the coordination between Zn^{2+} and supramolecular zwitterion, this electrolyte features a record-breaking ionic conductivity of 18.6 mS/cm, even at low temperatures of -40 °C (Fig. 5g). However, although supramolecular hydrogels provide the above advantages, their weak mechanical strength and poor processability limit their further application.

Double Network Polymer Hydrogels

Double network hydrogels consisting of covalent and noncovalent systems exhibit extraordinary mechanical properties [67]. The covalently cross-linked polymer network ensures that the hydrogel has sufficient strength and toughness, while the noncovalent cross-linked bonds dissipate energy during the loading process and improve the fatigue resistance and recovery of the double network hydrogel; this enables the requirements of high-performance flexible devices over a wide temperature range to be met (Fig. 6). The double network hydrogel possesses sufficient mechanical properties to satisfy the requirements of practical applications, due to its unique double network structure (Fig. 6a). In this respect, Sun et al. [68] simply applied covalently cross-linked polyelectrolyte-poly(2-acrylamido-2-methylpropanesulfonic acid potassium salt) and methyl cellulose to a concentrated alkaline solution and prepared an alkaline double network gel electrolyte that exhibited an extremely fast self-recovery ability and excellent fatigue resistance (Fig. 6b). In addition, the Zn-air battery assembled with this double network gel

electrolyte displayed a preeminent capacity retention when the temperature was lowered from 25 to -20 °C (Fig. 6c).

Ion transport kinetics are a key factor affecting electrolyte electrochemistry at low temperatures. Two effective strategies can be used to improve the ion transport rate: optimizing the dual network structure and constructing short-range ion transport channels. Zhang et al. [69] immersed an in situ polymerized PAM/cellulose nanofiber (CNF) precursor hydrogel in a mixture of KOH and KI to swell it to equilibrium and ultimately formed a novel double network hydrogel electrolyte (PAM-CNF/KOH/KI) (Fig. 6d). The hydration between K^+/I^- and water molecules significantly weakened the so-called "ice-like" HBs between the water molecules, thereby significantly lowering the crystallization temperature (Fig. 6e). Furthermore, as illustrated in Fig. 6f, the addition of CNF provided physical entanglement with PAM and formed an ion transport channel to improve the mechanical properties and ionic conductivity (Fig. 6g).

The design and fabrication of antifreeze hydrogel electrolytes for ARBs are based on the following principles: (1) the introduction of concentrated salt solutions, (2) the introduction of antifreeze organic additives, and (3) the synthesis or modification of hydrogels with charged or hydrophilic groups. Although these electrolytes are designed to further extend the low-temperature range of the electrolyte, it is not possible to solve the freezing problem using the hydrogel strategy alone due to the large pore sizes within the hydrogel [70]: As the pore size increases, the free water molecules play a dominant role, and the influence of polar groups on the polymer backbone are greatly diminished. The use of hydrogels in flexible device applications is extremely promising; however, special attention needs to be paid to the mechanical properties of quasi-solid hydrogels at sub-zero temperatures and to the freezing problem at low temperatures [71].

Electrolyte Additives

Electrolyte additives play a crucial role in enhancing battery performance without incurring additional production costs or altering the manufacturing process [72–75], and they can significantly improve the low-temperature performance of batteries due to their "low dose" and "fast acting" nature [76, 77]. Low-temperature aqueous electrolyte additives are often used to meet the requirements of a low melting point, miscibility with water, and high electrochemical and thermodynamic stability [78]. The use of some organic solvents (such as dimethyl sulfoxide (DMSO) [25], fluoroethylene carbonate (FEC) [79], glucose [80], 1, 3-dioxane (DOL) [81], and N, N-dimethylformamide (DMF) [82]) mixed with water in low-temperature aqueous batteries has been reported. Figure 7 shows that the electrochemical properties of the electrolyte can be effectively optimized at low
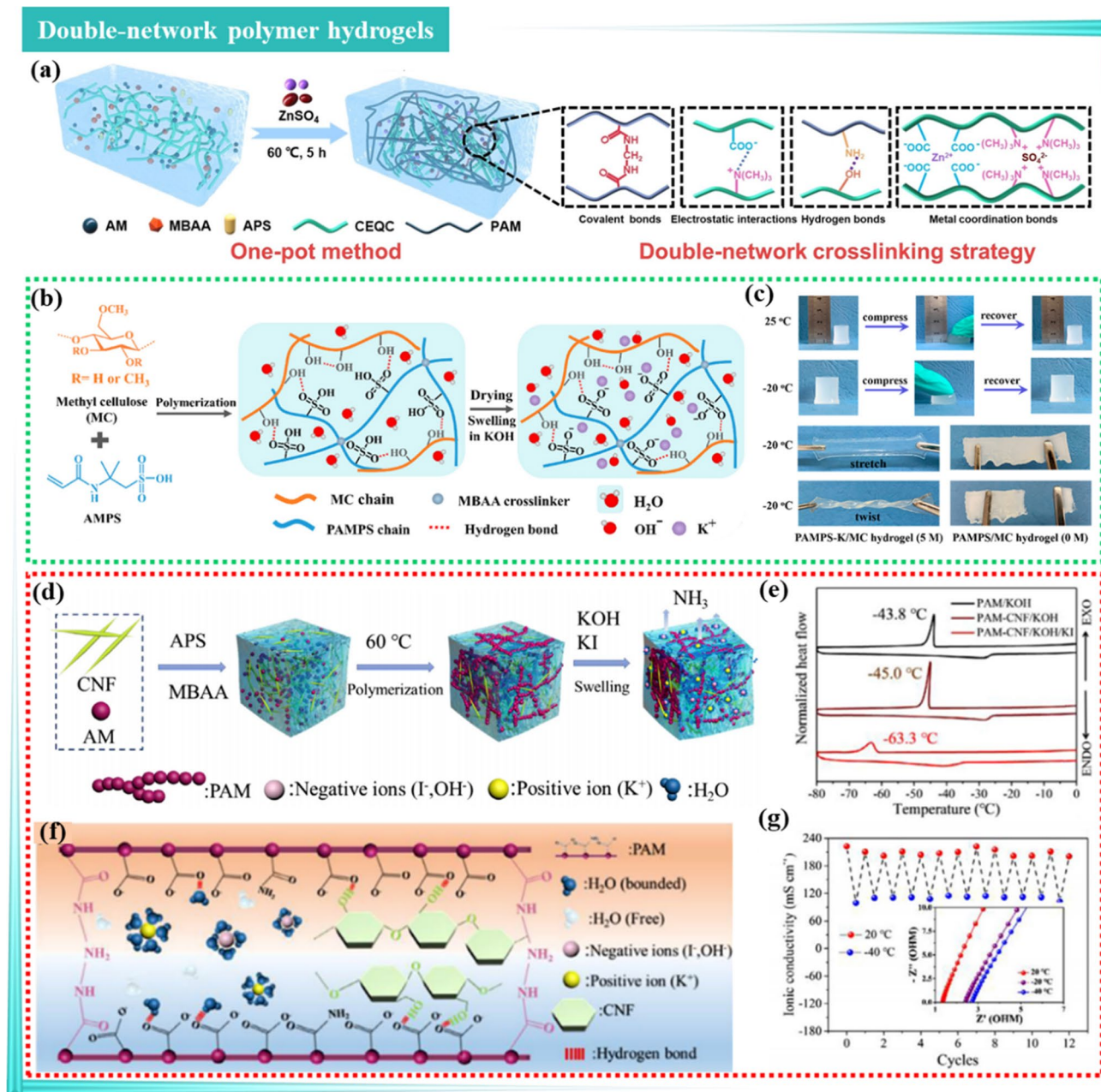
Fig. 6 **a** Schematic diagram of the structure of a double network hydrogel and the traditional synthesis method. Reproduced with permission from Ref. [67]. Copyright © 2003 Wiley. **b** Synthesis schematic of an alkaline double network gel electrolyte prepared by covalently cross-linked polyelectrolyte-poly (2-acryl amido-2-methyl propane sulfonic acid potassium salt) and methylcellulose **c** Chart demonstrating the mechanical properties of the alkaline double network gel electrolyte. **b** and **c** were reproduced with permission from Ref. [68]. Copyright © 2020 American Chemical Society. **d** Synthetic procedure used to prepare the double network hydrogel electrolyte (PAM-CNF/KOH/KI) by polymerization and swelling. **e** DSC results of PAM/KOH, PAM-CNF/KOH, and PAM-CNF/KOH/KI. **f** Diagram of the action mechanism of PAM-CNF/KOH/KI hydrogel electrolyte. **g** Ionic conductivity of PAM-CNF/KOH/KI hydrogel electrolyte and its stability at 20 and −40 °C. **d**, **e**, **f**, and **g** were reproduced with permission from Ref. [69]. Copyright © 2021 Elsevier

temperatures by introducing functional organic additives, such as antifreeze and buffering agents.

EG is a widely used antifreeze agent [88]; the hydroxyl groups in EG can form strong HBs with water molecules, and this disrupts the hydrogen-bonding network among water molecules, inhibits the formation of ice crystals, and effectively reduces the freezing point of the electrolyte. In addition, EG is cheap, has good water solubility, a high dielectric constant (Eq. (3)), and a high flash point, which makes it a promising solvent additive for electrolytes. Tron
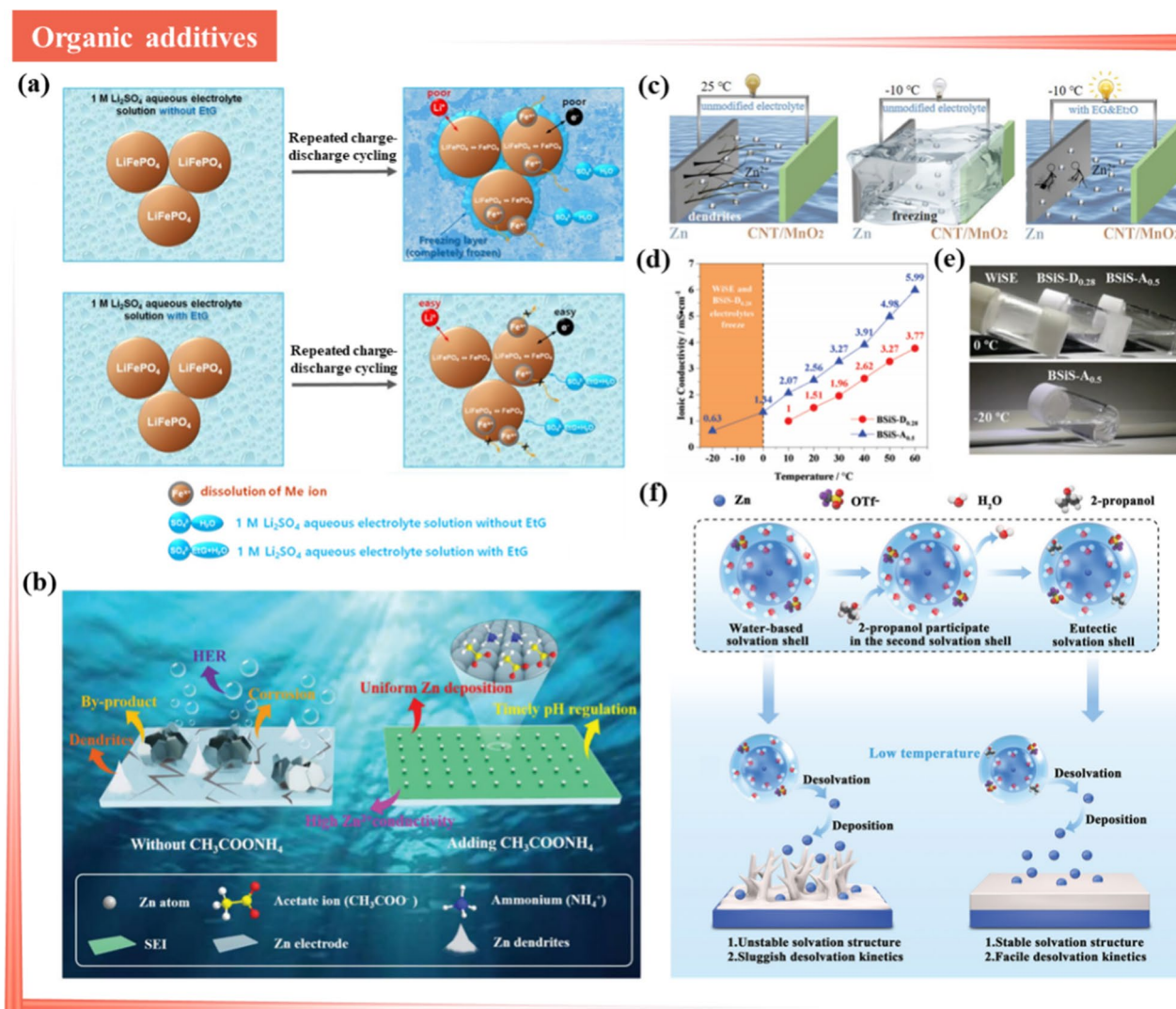
Fig. 7 a Schematic illustration of the LiFePO$_4$ material's particles in a 1 mol/L Li$_2$SO$_4$ aqueous electrolyte solution without and with the addition of antifreeze EG during cycling at low temperatures. Reproduced with permission from Ref. [83]. Copyright © 2019 American Chemical Society. **b** Schematic illustration of Zn surface evolution in electrolytes with/without CH$_3$COONH$_4$ additive. Reproduced with permission from Ref. [84]. Copyright © 2022 Wiley. **c** Schematic illustration showing the superiority of the electrolyte modified in this study. Reproduced with permission from Ref. [85]. Copyright © 2021 Elsevier. **d** Ionic conductivity of BSiS-D$_{0.28}$ and BSiS-A$_{0.5}$ hybrid electrolytes at a temperature range of −20 to 60 °C. **e** Photographs showing the states of WiSE, BSiS-D$_{0.28}$, and BSiS-A$_{0.5}$ electrolytes at 0 and −20 °C. **d** and **e** were reproduced with permission from Ref. [86]. Copyright © 2022 Elsevier. **f** Structure of eutectic solvation structure and the Zn^{2+} deposition process at low temperature. Reproduced with permission from Ref. [87]. Copyright © 2022 Wiley

et al. [83] used EG antifreeze additives to improve the low-temperature performance of rechargeable lithium-sulfur (Li–S) ion batteries (Fig. 7a); the antifreeze agent was found to expand the temperature range of the aqueous solution, improve the kinetics of the active material, and reduce the polarization resistance under charge and discharge cycles. Ethyl ether (Et$_2$O) is also an effective electrolyte antifreeze additive that helps to improve the low-temperature performance of ARBs, extend their temperature range, and improve their cycling performance. In the study of Wang et al. [85], a conventional electrolyte for aqueous Zn∥MnO$_2$

cells (consisting of a 2 mol/L ZnSO$_4$ + 0.2 mol/L MnSO$_4$ aqueous solution) was optimized by incorporating Et$_2$O and EG as additives (Fig. 7c). The cycling performance of the Zn∥MnO$_2$ cells was improved with the addition of Et$_2$O, and it played a role in inhibiting the growth of Zn dendrites. The cells with an EG/30% + Et$_2$O/1% electrolyte showed the highest capacity retention and the best cycling performance at −10 °C and 3 A/g compared to those without the additive.

In recent years, the physical solubility limit of salt in water has been broken by the addition of acetate ions, and non-polarizing protons prevent the overgrowth and

precipitation of ionic oligomers [89, 90]. Lin et al. [84] found that the addition of CH_3COONH_4 additive to the conventional $ZnSO_4$ electrolyte resulted in the stable cycling of the Zn‖Zn symmetric cell at −10 °C (Fig. 7b),

According to Bjerrum's treatment (Eq. (3)), the critical distance for ion pair formation q can be described as,

$$q = \frac{|z_i z_j| e^2}{8\pi\varepsilon\varepsilon_0 kT} \tag{3}$$

where q is the critical distance for the ion pair formation; i and j are the species of ions; z is the valence order of ions; and ε, ε_0, and k are the dielectric constant of the solvent, the dielectric constant of solvent at vacuum, and Boltzmann's constant, respectively. As the temperature drops, the larger q of the ion pair formation relates to the tendency of the anions and cations to associate more easily, and n_i then decreases.

Following the Stokes–Einstein equation (Eq. (4)), the increased viscosity (η) of the electrolyte also needs to be addressed at low temperatures,

$$D = \frac{kT}{6\pi\eta r} \tag{4}$$

where D, r, and T are the diffusion constant, the solvation radius, and the temperature, respectively, and η and r are inversely proportional to ionic mobility, μ_i [29].

Chen et al. [86] reported an advanced hybrid electrolyte with the introduction of acetonitrile (AN) as a co-solvent in a 15.3 mol/L LiTFSI salt electrolyte, which exhibited an electrochemical stability window of 4.5 V. The low viscosity of AN allowed the BSiS-A$_{0.5}$ electrolyte to maintain sufficient ionic conductivity at low temperatures, remaining in a liquid state even at −20 °C (Fig. 7d, e). The $LiMn_2O_4$‖$Li_4Ti_5O_{12}$ (LMO/LTO) full cell using BSiS-A$_{0.5}$ maintained a discharge capacity of 110 mAh/g after 120 cycles at 0 °C.

Due to the slow reaction kinetics, the electrochemical performance of ARBs severely deteriorates at low temperatures, and recent studies have shown that modulating the solventized structure of the aqueous electrolyte is an excellent strategy that can be employed to ameliorate this. Ma et al. [87] proposed the concept of a "eutectic solvation shell layer" for the ex-solvation shell layer of Zn^{2+} composed of 2-propanol. With the addition of alcohols of different carbon chain lengths and isomers, the alcohol molecules can modulate the ex-solvation shell layer by replacing water molecules to build a eutectic layer (Fig. 7g). Due to the structural advantages of the eutectic solventized shell, 150 mAh Zn‖V_2O_5 soft pack batteries can provide remarkable performances at low temperatures of −20 °C. This study demonstrated a new strategy that can be employed to achieve fast charging and long-term cycling capability of ARBs under extreme conditions.

Figure 8 shows that introducing electrolyte additives with organic groups that inhibit the formation of HBs is also an effective way of lowering the freezing point [91, 92]. Organic solvents containing the elements F, O, and N (alcohols, ethers, sulfones, esters, amides, nitrile) bond more strongly to water molecules and break HBs more easily, thus lowering the freezing point. Butyl sulfone is chosen for its low toxicity, high miscibility with water, high oxidative stability, and strong interactions with water molecules, and as such, it has been utilized as a co-solvent in electrolytes [93]. For example, Liu et al. [94] employed butyl sulfone to actively participate in the solvation sheath of Li ions, where its presence reinforced the O–H bonding of water and significantly disrupted the H-bonding network (Fig. 8a). The $LiMn_2O_4$‖$Li_4Ti_5O_{12}$ full cell, using the hybrid electrolyte, exhibited an outstanding performance at −20 °C, demonstrating a high voltage (2.7 V) and a Coulomb efficiency of 98% (Fig. 8b).

Attention also needs to focus on the combined use of organic solvents and water and on the number of HB donors and acceptors for the solvents. In this respect, Zhao et al. [95] employed NMP (N-methyl-2-pyrrolidone) molecules as end-cap reagents to hinder proton conduction in aqueous electrolytes. The NMP structure comprises an HB acceptor but lacks an HBs donor site, which effectively impedes HB propagation and restricts the pathway for proton transport in aqueous electrolytes (Fig. 8c). This electrolyte provides excellent low-temperature performance due to the end-capping of HBs.

Insufficient ionic conductivity and freezing of the electrolyte are considered to be the main limitations for storing electrochemical energy at a low temperature. Nian's group [25] reported an electrolyte with DMSO as an additive that had a freezing point lower than 130 °C, and MD simulations were used to understand the underlying mechanism behind the low freezing point of the electrolyte. Figure 8d, e illustrates that in the mixed water/DMSO electrolyte, an HB network is formed through the interaction between oxygen atoms in the S=O bond of DMSO and the hydrogen atoms in the O–H bond of water. When the temperature drops below 0 °C, the intermolecular HBs between DMSO and water impede the formation of the tetrahedral structure of ice, thereby enabling the electrolyte to exhibit low-temperature tolerance.

Most of the studies mentioned above employed high-polarity molecules with large additive dosages. However, the involvement of bulk organic molecules in a primary solvation sheath (PSS) inevitably enlarges the de-solvation penalty. By introducing low-polarity 1, 2-dimethoxyethane (DME) into dilute 1 mol/L trifluoromethanesulfonic acid ($Zn(OTf)_2$) aqueous solution, Dong et al. [96] designed a cell-core structured electrolyte. The electrolyte was
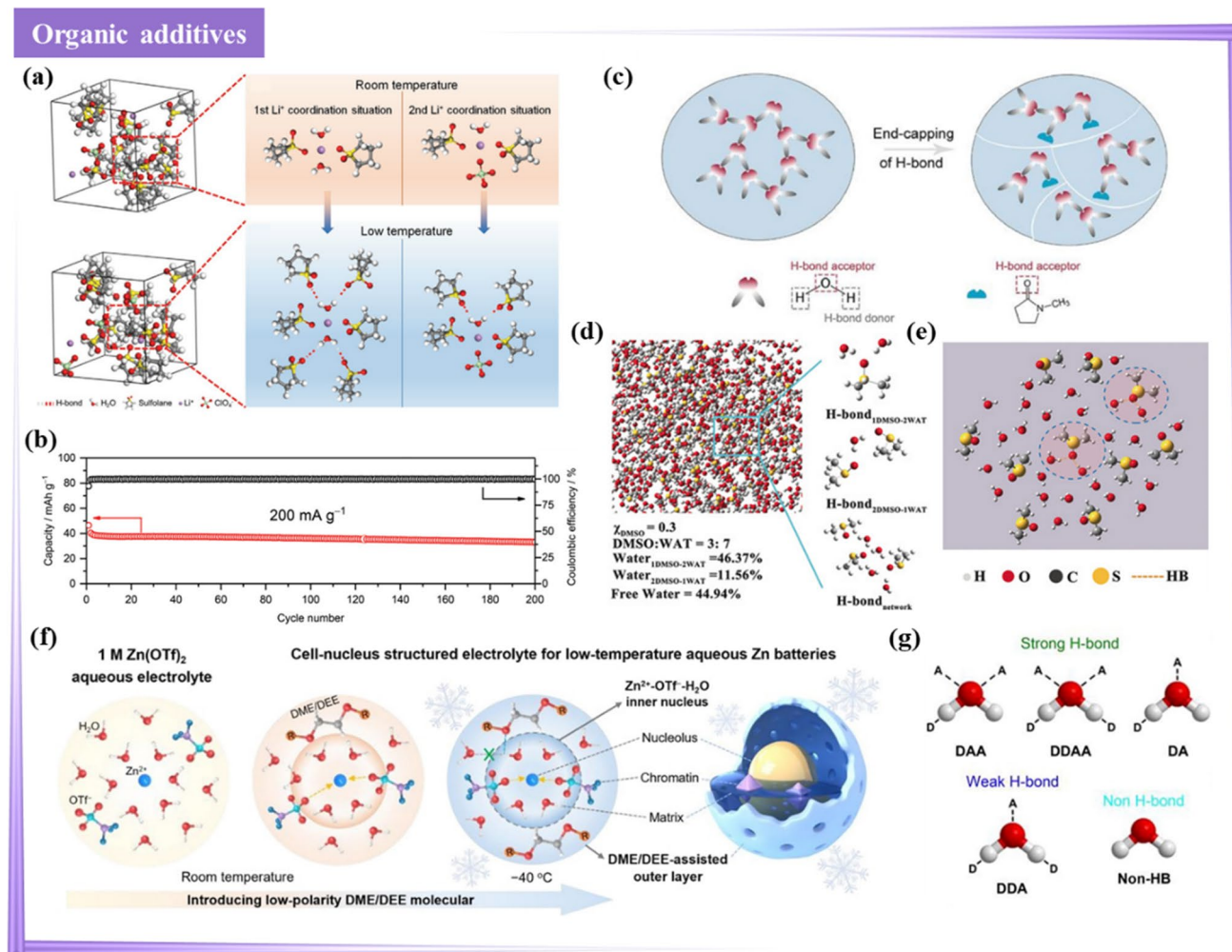
Fig. 8 **a** MD simulations of 12SL–4H$_2$O–3LiClO$_4$ electrolyte. **b** Cycling stability and CE of LMO/LTO full battery using 12SL–4H$_2$O–3LiClO$_4$ electrolyte at −20 °C. **a** and **b** were reproduced with permission from Ref. [94]. Copyright © 2022 Wiley–VCH Verlag. **c** Schematic diagrams for end-capping of the H-bond network in an aqueous solvent by employing an NMP molecule that possesses an H-bond acceptor but no H-bond donor. Reproduced with permission from Ref. [95]. Copyright © 2023 Elsevier. **d** Conforma-

tion analysis of the system with DMSO=0.3 from MD simulations. **e** Local structure of the DMSO=0.3 system from MD simulations. **d** and **e** were reproduced with permission from Ref. [25]. Copyright © 2019 Wiley. **f** Schematic illustration of cell-nucleus structured electrolyte design for low-temperature aqueous Zn batteries. **g** Schematic modes representing H$_2$O molecule with DAA, DDAA, DA, DDA, and non-HB. **f** and **g** were reproduced with permission from Ref. [96]. Copyright © 2023 Elsevier BV

characterized by an inner core composed of an OTf-rich Zn^{2+}-PSS and an outer layer consisting of a DME-modulated Zn^{2+}-external solvation sheath (Fig. 8f). The addition of DME improved the Zn-OTf$^-$ coordination without participating in the Zn^{2+}-PSS, thereby facilitating favorable reaction kinetics at ultra-low temperatures. Furthermore, DME disrupted the original hydrogen-bonding network of water, effectively reducing the electrolyte's freezing point (Fig. 8g). This unique nucleus-like structure provided an ultra-low freezing point (−52.4 °C), high ionic conductivity (1.06 mS/cm at −40 °C), and the formation of a robust ZnF$_2$-rich solid electrolyte interface (SEI) on the surface of the Zn electrode.

The physicochemical properties of the solvent have a considerable influence on the performance of aqueous batteries over a wide temperature range. It is evident from several methods presented above that theoretical simulations and corresponding statistical analyses can be used to obtain the relevant properties of the solvent structure, and numerous theoretical models have been developed to obtain associated information. More encouragingly, with the development of machine learning (ML) predictions, ML models can be trained based on limited MD results to construct quantitative relationships between the electrolyte formulations and the corresponding physicochemical properties [97].

Instead of adding flammable and toxic organic antifreeze additives to improve the low-temperature performance, it makes scientific sense to add common inexpensive inorganic inert additives. Certain ionic additives that contain multivalent cations have the ability to form strong interactions with water molecules and effectively lower the freezing point of aqueous solution electrolytes. Research conducted by Sun et al. and Zhu's team [98–100] demonstrated the use of antifreeze double-cation electrolytes to improve the low-temperature performance of aqueous electrolyte systems. In this respect, Sun et al. [98] reported an antifreeze double-cation electrolyte with 3.5 mol/L $Mg(ClO_4)_2$ + 1 mol/L $Zn(ClO_4)_2$. By introducing the oxygen ligands, Mg^{2+} and ClO_4^-, the proportion of HBs in the water molecules was significantly reduced, and theoretical calculations confirmed

the synergistic effect of cations and anions on freezing point reduction (Fig. 9a, b). The dissolution of $Mg(ClO_4)_2$ in water is a violent exothermic process, and it indicates that the bonding energy between Mg^{2+} and O atoms is higher than the bonding energy of HBs (Fig. 9c). Therefore, Mg^{2+} is more likely to combine with O atoms in water and break the arrangement of HBs to form stable hydrated ions, while ClO_4^- as the HB receptor can form weak HBs with H atoms in H_2O. By simultaneously regulating the chemical environment of O and H atoms in H_2O, the electrolyte obtained an ultra-low freezing point of 121 °C (Fig. 9d). Zhu's team [99] reported an electrolyte system that operated at low temperatures by introducing 3.5 mol/L $Mg(ClO_4)_2$ into a 0.5 mol/L $NaClO_4$ electrolyte. Mg^{2+} has a significant effect on the chemical environment of water molecules; it can effectively
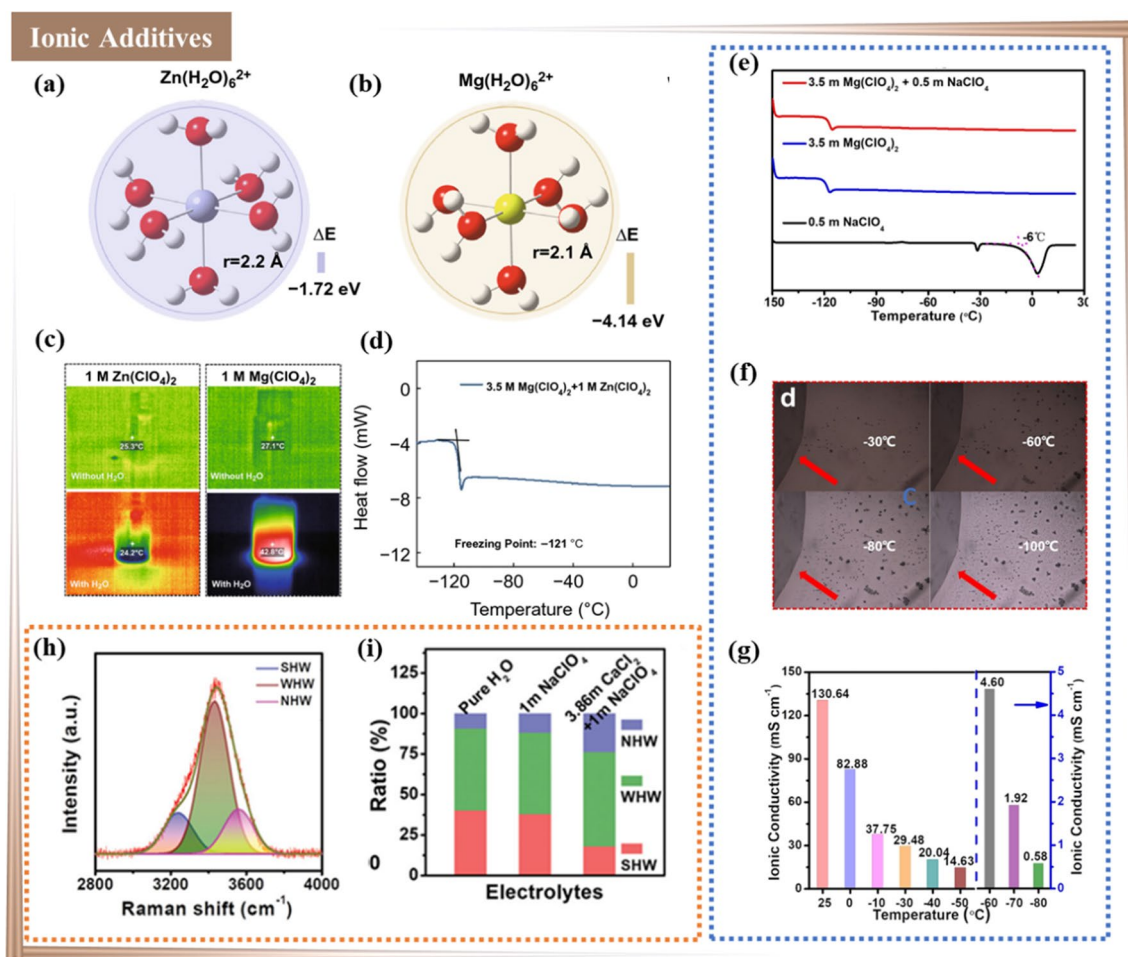

Fig. 9 Calculated formation energy and hydrated radius of a Zn^{2+} solvation configuration. b Mg^{2+} solvation configuration. c Photographs of infrared thermometry of different electrolytes. d DSC curve of 3.5 mol/L electrolyte. a, b, c, and d were reproduced with permission from Ref. [98]. Copyright © 2021 Springer Singapore. e DSC results (from −150 to 30 °C with a heating rate of 5 °C/min) of various electrolytes. f Polarizing microscope observation of the 3.5 mol/L $Mg(ClO_4)_2$ + 0.5 mol/L $NaClO_4$ electrolyte during the cooling process. g Ionic conductivity of 3.5 mol/L $Mg(ClO_4)_2$ + 0.5 mol/L $NaClO_4$ electrolyte at different temperatures. e, f, and g were reproduced with permission from Ref. [99]. Copyright © 2022 Wiley. h Fitted O–H stretching vibration in the Raman spectra of 3.86 mol/L $CaCl_2$ + 1 mol/L $NaClO_4$ electrolyte. i Component proportions of water with different HBs for $NaClO_4$-based electrolytes. h and i were reproduced with permission from Ref. [100]. Copyright © 2022 Wiley

attract water from the water clusters, which changes the initial hydrogen-bonding network and finally lower the freezing point of the electrolyte. As shown in Fig. 9e, f, the freezing point of the mixed electrolyte was significantly reduced, and no salt precipitation or ice crystals were observed during the cooling process. This mixed electrolyte was also found to have a high ionic conductivity of 4.86 mS/cm at -60 °C (Fig. 9g). The synergistic effect between cations and anions enabled the electrolyte to achieve an ultra-low freezing point.

In addition to $Mg(ClO_4)_2$, $CaCl_2$ and $NaClO_4$ have been used in electrolyte systems, and their abilities to lower the freezing point and improve the low-temperature performance have been demonstrated [100]. Low-cost $CaCl_2$ was used as an antifreeze added to the electrolyte of 1 mol/L $NaClO_4$ aqueous solution, and Raman spectroscopy clearly showed that $CaCl_2$ strongly interacted with the water molecules and regulated the ratio of HBs in the electrolyte, thereby significantly lowering the freezing point of the optimized electrolyte (Fig. 9h, i). These inorganic antifreeze additives offer advantages over toxic and flammable organic co-solvents, and they provide a safer and more cost-effective approach for developing high-performance cryogenic water-based cells.

For future practical applications, the ideal additive or co-solvent needs to be capable of improving the low-temperature performance of aqueous electrolytes and also ensuring a stable interface for the metal ions phase to protect the long-term cycling of the metal anode. The formation of stable HBs between additives or co-solvents and water molecules is crucial for designing antifreeze water electrolytes [101]. Organic additives play an important role in constructing SEI that can effectively adapt to low-temperature environments, and they combine the advantages of both aqueous and non-aqueous solvents [102]. However, organic additives are toxic, and the addition of organic additives has a significant effect on the ionic conductivity of the electrolyte. There is also a continuing need to research safe organic and non-polluting inorganic additives that achieve a low-temperature performance without compromising the unique safety characteristics of ARBs.

Aqueous Rechargeable Battery (ARB) at High Temperatures

Compared to organic batteries, aqueous batteries deliver excellent thermal safety. The rise in temperature increases the ionic conductivity of the electrolyte, and the battery capacity increases accordingly. However, although aqueous electrolytes are a favorable choice for non-flammable batteries, most electrolytes suffer from poor stability at high temperatures due to the enhanced activity of water molecules. The high temperature inside the cell accelerates the

water-induced side reactions of both electrodes, which may lead to structural damage, a phase change of the cathode, and depletion of the metal anode [103, 104]. Therefore, the next section discusses employing an electrolyte modification strategy for highly stable ARBs at a high temperature.

Concentrated Electrolytes

Concentrated electrolytes can inhibit electrolyte volatilization, and employing "water-in-salt" electrolytes (WiSEs) is an effective strategy for improving the high-temperature performance of ARBs. The concentration of ions in WiSEs is much higher than the moisture content, and this gives the electrolyte a wide liquid-state temperature range and a stable electrochemical window (Fig. 10). Jiang et al. [105] used 22 mol/L KCF_3SO_3 with a wide voltage window (3 V), which inhibited the dissolution effect and provided high conductivity and low viscosity (Fig. 10a). Furthermore, the KFeMnHCF-3565‖22 mol/L KCF_3SO_3‖PTCDI soft pack cells exhibited a superior performance at a low rate (0.5 C/0.1 C) and over a wide temperature range (-20 °C to 60 °C) (Fig. 10b). Zhang et al. [106] proposed a new sodium-ion aqueous battery using a 17 mol/L $NaClO_4$ electrolyte. The "water-in-salt" electrolyte had a low freezing point of -31.3 °C and boasted high thermal stability reaching 200 °C (Fig. 10c). The complete cell benefited from the low freezing point and high thermal stability of the "water-in-salt" electrolyte and operation over a wide temperature range of -40 °C to 100 °C was achieved (Fig. 10d), evidencing typical all-climate operation. Xia's group [107] reported a NiHCF@CNTs‖poly(1,5-NAPD) ammonium-ion battery with a 19 mol/kg CH_3COONH_4 electrolyte (Fig. 10e) that provided a high boiling point (140 °C) and a low freezing point (-38 °C) and allowed the ammonium-ion battery to operate over a wide temperature range (-40 to 80 °C) (Fig. 10f).

Solvent Modification of Electrolyte

Solvent modification of the electrolyte is an effective strategy used to inhibit a drastic water-induced side reaction and dendrite growth on the metal electrode surfaces at high temperatures. Generally, solvent additives improve the thermal stability of ARBs in the following two ways (Fig. 11): (1) preferential reduction on the electrode surface to form a highly thermally stable SEI; (2) participation in the construction of solventized structures and reconfiguration of the HB network of water, which reduces the content and activity of water and inhibits the violent decomposition of water molecules at high temperatures. Xiong et al. [82] modified the $ZnSO_4$ electrolyte with a polar aprotic N, N-dimethylformamide ($ZnSO_4$–H_2O–DMF) (Fig. 11a), which reached a boiling point of 82 °C (Fig. 11b) and in situ formed a
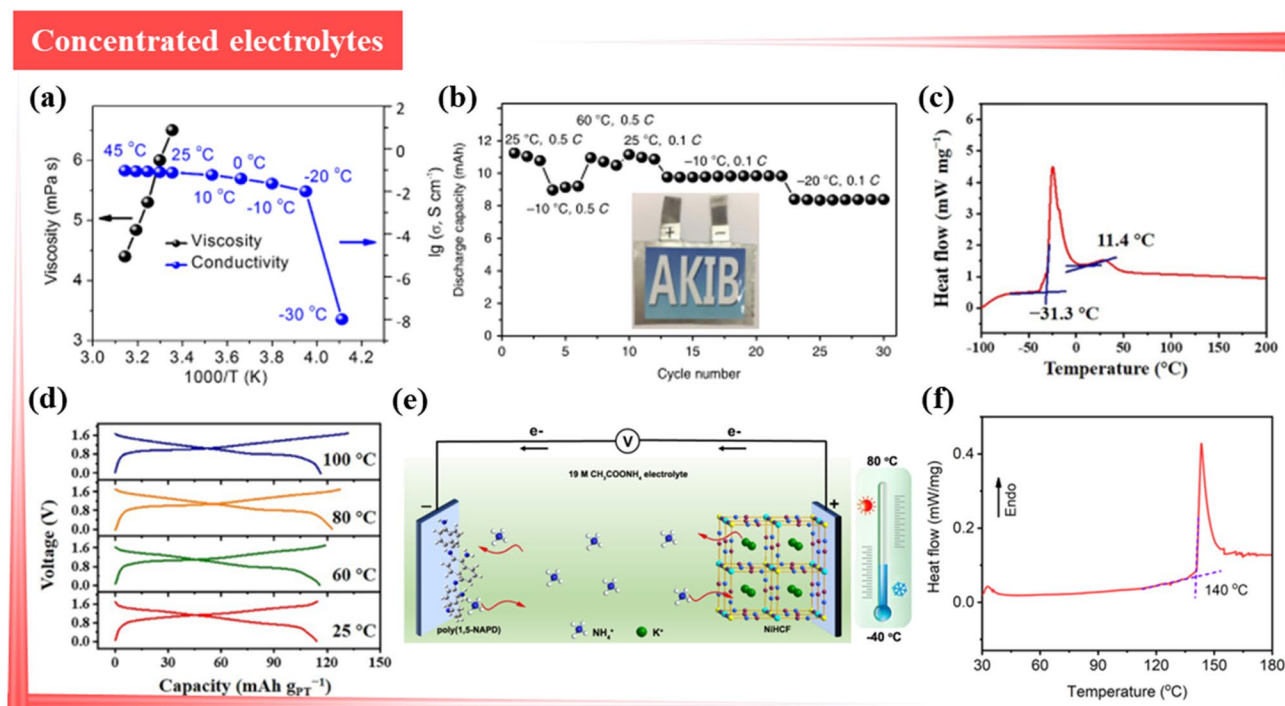
Fig. 10 a Viscosity and conductivity at different temperatures for the 22 mol/L KCF$_3$SO$_3$ electrolyte. **b** Cycling performance of the KFeM-nHCF-3565‖22 mol/L KCF$_3$SO$_3$‖PTCDI pouch cell at different rates (0.5℃ and 0.1℃) and temperatures (− 20 °C, − 10 °C, 25 °C, and 60 °C) from 0 to 2.3 V. **a** and **b** were reproduced with permission from Ref. [105]. Copyright © 2021 American Chemical Society. **c** DSC measurement of the 17 mol/kg NaClO$_4$ electrolyte. **d** Galva-nostatic discharge–charge curves of the NiHCF‖PT full cell from 25 to 100 °C at 5 A/g$_{PT}^{-1}$ **c** and **d** were reproduced with permission from Ref. [106]. Copyright © 2022 Elsevier. **e** Schematic of the energy storage mechanism of ammonium-ion batteries at high temperature. **f** DSC measurement of 19 mol/L CH$_3$COONH$_4$ electrolyte. **e** and **f** were reproduced with permission from Ref. [107]. Copyright © 2021 Elsevier

Zn^{2+}-conducting Zn$_5$(CO$_3$)$_2$(OH)$_6$ SEI on the electrode surface during the cycling process. The Zn$_5$(CO$_3$)$_2$(OH)$_6$ SEI features high thermal stability due to its high thermal decomposition temperature of 250 °C (Fig. 11c), enabling it to inhibit dendrite formation at high temperatures of 70 °C. Molecular crowding is a common phenomenon in living cells where water activity is substantially suppressed by molecular crowding agents through altering the hydrogen-bonding structure [108]. Wang et al. [109] formulated a crowding agent where 1, 5-pentanediol (PD) was introduced into an aqueous electrolyte. MD simulations revealed that at 100 °C, the PD expelled a large amount of H$_2$O from the Zn^{2+} solventized sheath (Fig. 11d); this modified the Zn^{2+} solventized structure and enhanced the O–H bonding of H$_2$O to inhibit the reactivity of water and broaden the stable voltage window of the electrolyte to 2.35 V (Fig. 11e) while maintaining the high flame retardancy (Fig. 11f) and thermal stability of the electrolyte.

Hydrogels Electrolytes

Water is retained in the hydrogel structure, and hydrogels can, therefore, also be used in high-temperature applications.

However, the introduction of highly concentrated salt solutions and solvent additives is typically necessary to mitigate water loss and improve the safety of hydrogels at extremely high temperatures (Fig. 11). Gu et al. [110] designed a highly stretchable and temperature-resistant hydrogel electrolyte with a guanosine G-quadruplexes, small-molecule-based, supramolecular, polymer binary network (SP-DN) structure (Fig. 12a). The developed SP-DN hydrogel electrolytes were based on a concentrated KOH aqueous solution and consisted of a series of guanosine G-tetramers interpenetrated with PAM networks. The obtained KOH (6 mol/L)-filled SP-DN hydrogels exhibited hyper stretchability (> 1600%), a wide temperature tolerance (from − 196 to 100 °C) (Fig. 12b), excellent interfacial adhesion, and ultra-high low and high-temperature conductivity (252.2 mS/cm at − 50 °C, 431.7 mS/cm at 100 °C) (Fig. 12c). Replacing water with a solvent that has a high boiling point is one way of reducing the volatility of the electrolyte. Zheng et al. [111] prepared rigid, noncombustible, spirocyclic, pentaerythritol diphosphate-based, cross-linked gel polymer electrolytes (SPDPA) by in situ thermal polymerization. The electrolyte offered favorable interfacial compatibility and thermal stability (Fig. 12d), and as shown in Fig. 12e, the addition of SPDPA effectively increased the nonflammability
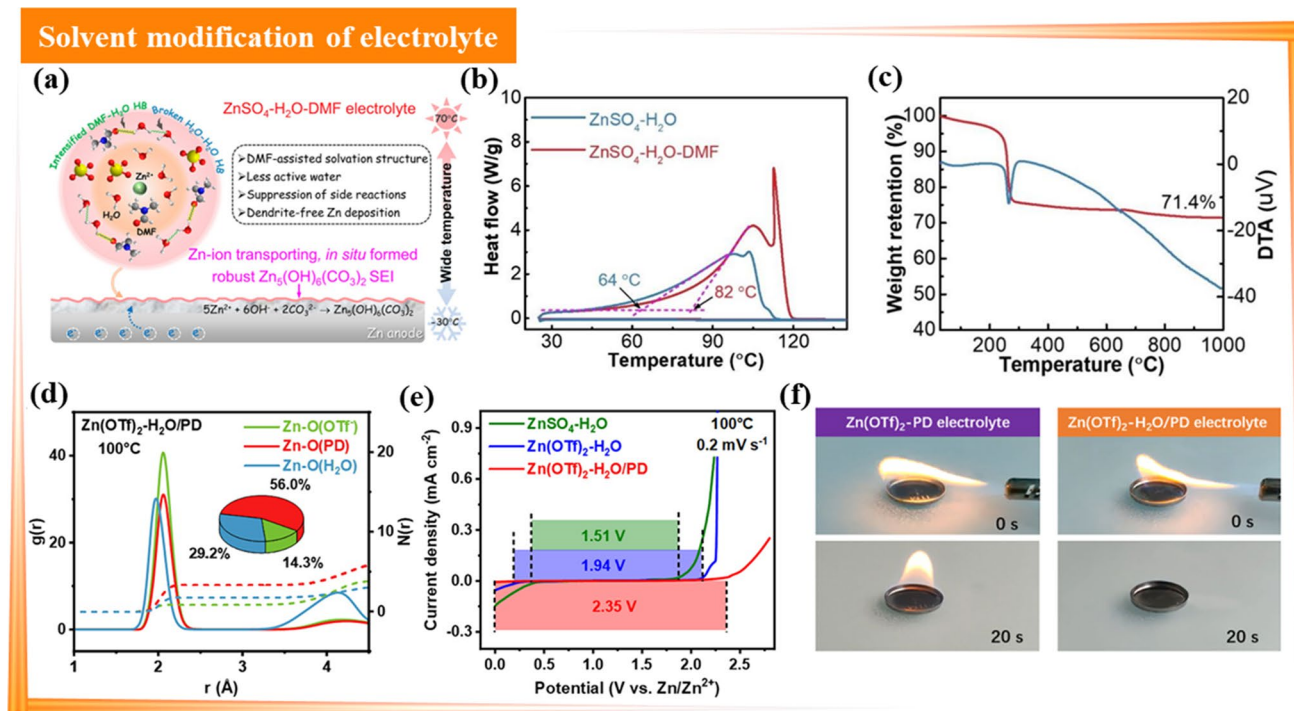
Fig. 11 **a** Schemes illustrating the different reaction processes of the Zn^{2+} solvation structure and corresponding interfacial interaction between the Zn anode surface and electrolyte under $ZnSO_4$–H_2O–DMF electrolytes. **b** DSC measurement of $ZnSO_4$–H_2O–DMF electrolytes from 25 to 150 °C. **c** Thermogravimetry analysis (TGA) curves of the as-synthesized $Zn_5(OH)_6(CO_3)_2$. **a**, **b**, and **c** were reproduced with permission from Ref. [82]. Copyright © 2023 American Chemical Society. **d** The racial distribution functions of $Zn(OTf)_2$–H_2O/PD electrolyte at 100 °C obtained via MD calculations. **e** Linear sweep voltammetry results of $ZnSO_4$–H_2O, $Zn(OTf)_2$–H_2O, and $Zn(OTf)_2$–H_2O/PD electrolyte. **f** Flammability tests of different electrolytes with/without PD solvent. **d**, **e**, and **f** were reproduced with permission from Ref. [109]. Copyright © 2022 American Chemical Society

of the electrolyte. The NVP‖GPE‖Na full cell operated at a constant current density of 270 mA/g for 200 cycles at a high temperature of 60 °C and with a discharge specific capacity of 93.4 mAh/g (Fig. 12f). Hyun et al. [112] developed high-modulus ion-conductive gel electrolytes using imidazolium ionic liquids and exfoliated hexagonal boron nitride (hBN) nanoplates. The high thermal stability of the hBN nano-solid matrix facilitated the high operation rate of solid-state rechargeable Li-ion batteries at high temperatures reaching 175 °C (Fig. 12g). In addition, using both GL additives and freeze–thawing techniques, Jiang et al. [113] designed a "hydrogen bond-microstructure" dual-regulated, low-temperature-resistant, stretchable gel electrolyte (HG-F) (Fig. 12h). The freeze–thaw method allowed the PVA molecular chains to interact with each other and twist to form a three-dimensional cross-linked structure tightly bound by van der Waals and HBs, which greatly reduced the number of free water molecules and resulted in stability of the HG-F gel electrolyte over a wide temperature range. Furthermore, Hou et al. [114] reported a novel "water-in-eutectogel (WiETG)" electrolyte prepared by swelling a hydrogel polymer with a low water content DES. The three stages of weight loss that occurred are shown in Fig. 12i and are related to the evaporation of

water (< 120 °C), the decomposition of acetamide or polymer species (120–400 °C), and the decomposition of LiTFSI (> 400 °C). The WiETG exhibited high thermal stability over a wide temperature range. Data about the electrochemical properties applicable to wide temperature domain electrolytes are presented in Table 1 [115–132].

To meet the requirements of safe and long-term cycling above room temperature, the main principle of high-temperature electrolytes is to improve thermal stability by reducing volatility and controlling decomposition. By decreasing the water content, the boiling point of the electrolyte can be increased, and various methods (such as those involving the use of high concentrations, organic/water hybrid solvents, and hydrogels) have been established based on this principle. To further enhance the high-temperature resistance of the electrolyte, the salt needs to have high thermal stability (resistance to decomposition at high temperatures). In addition, organic cathodes may dissolve in organic solvent-based electrolytes, while some inorganic cathodes may dissolve or decompose at high temperatures [133, 134]. In addition to electrolyte modification, our previously works demonstrate that the wide temperature range performance can also be improved by designing and modifying the electrode
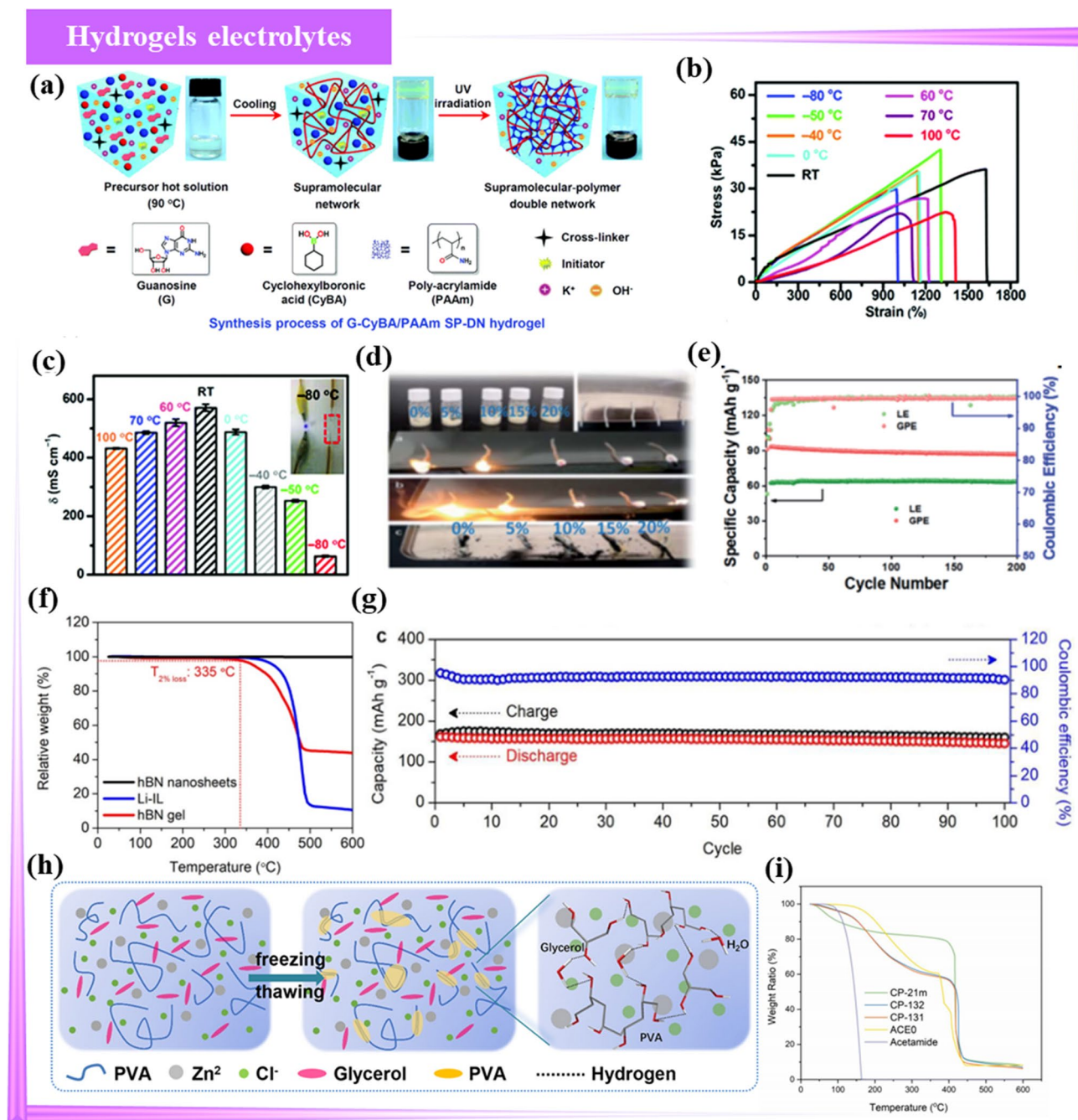
Fig. 12 a Schematic diagram of synthesis method and polymerization mechanism, and digital images of small molecule-based SP-DN hydrogel electrolytes. b Compressive stress–strain results of the G-CyBA/PAAm SP-DN and the PAAm SN hydrogels with various soaking times in aqueous KOH (6 mol/L) at temperatures from −80 to 100 °C. c Digital images of stretchability and conductivity of the 6 mol/L KOH-filled SP-DN hydrogel electrolytes at temperatures from −80 to 100 °C. a, b, and c were reproduced with permission from Ref. [110]. Copyright © 2021 Royal Society of Chemistry. d Burning and residue of cotton fiber wicks soaked with LE with different flame-retardant content. e Cycling performances and coulombic efficiency of the NVP/Na cells at 60 °C. f TGA curves of hBN gel electrolytes. d, e, and f were reproduced with permission from Ref. [111]. Copyright © 2020 Royal Society of Chemistry. g Cycling performance of the cell tested at 10°C at 175°C. Reproduced with permission from Ref. [112]. Copyright © 2019 American Chemical Society. h Schematic diagram of the fabrication process and principle. Reproduced with permission from Ref. [113]. Copyright © 2023 Wiley. i TGA curves of CP-131, CP-132, and CP-21 m. Reproduced with permission from Ref. [114]. Copyright © 2022 Wiley

Table 1 Summary of different electrolytes for operating at wide temperatures

Category	Electrolyte	Ionic conductivity (mS/cm)	Freezing point (℃)	Operating temperature range (℃)	Systems	Capacity (mAh/g)	Current density	T (℃)	References
High-concentration electrolytes	7.5 mol/L $ZnCl_2$/H_2O	1.79(60 °C)	− 144	− 90–60	Zn | PANI	50.6 187.7	0.01 A/g	− 90 60	[24]
	3 mol/L LiCl/4 mol/L $ZnCl_2$/H_2O	*	*	− 10–50	Zn | $LiFePO_4$	93.8	102 mA/g	− 10	[131]
	22 mol/L KCF_3SO_3/H_2O	*	− 39	− 30–25	PTCDI | δ-$K_{0.5}V_2O_5$	3.4	5 C	− 30	[44]
	25 mol/L NaFSI/10 mol/L NaFTFSI/H_2O	11.8(30 °C)	− 34	− 10–30	$NaTi_2(PO_4)_3$ | $Na_3(VOPO_4)_2F$	65 80	0.5 C 1 C	− 10 30	[48]
	4 mol/L $Zn(BF_4)_2$/H_2O	1.47(− 70 °C)	− 122	− 95–25	Zn | TCBQ	63.5 101.4	0.1 C	− 95 − 30	[49]
	17 mol/L $NaClO_4$/H_2O	4.4(− 40 °C)	− 31.3	− 40–100	PT | NiHCF	85.6	0.5 A/g_{PT}	− 40	[106]
	19 mol/L CH_3COONH_4/H_2O	*	− 38	− 40–80	poly(1,5-NAPD) | NiHCF@CNTs	130 102	0.05 A/g 4 A/g	− 40 80	[107]
	7.6 mol/L $ZnCl_2$/H_2O	8.21(RT)	*	− 35–60	Zn | NaV_3O_8·1.5H_2O	194	1 A/g	− 35	[118]
	3.5 mol/L $Mn(ClO_4)_2$/H_2O	*	− 122	− 70–25	Polyaniline | CF@MnO_2	53	0.3 C	− 70	[122]
Hydrogels electrolyte	1 mol/L $Zn(CF_3SO_3)_2$/PVA/glycerol/H_2O	10.7(− 30 °C)	*	− 30–60	Zn | δ-MgVO	490.2 256.3	2 A/g	60 − 30	[60]
	$Zn(BF_4)_2$/PAM/H_2O	*	*	− 70–25	Zn | PANI@SWCNTs	45.4	50 mA/g	− 70	[61]
	IL-OH/(DHPMIm)Cl/H_2O	0.08(− 80 °C)	*	− 80–20	$LiTi_2(PO_4)_3$@C | AC	43	0.1 C	− 80	[62]
	7.5 mol/L $ZnCl_2$/H_2O/PSA	15.6(− 60 °C)	*	− 60–25	Zn | AC	40.7	0.5 A/g	− 60	[65]
	5 mol/L KOH/H_2O/PAMPS/MC	105(25 °C)	− 30	− 20–25	Zn | air	754.2	1 mA/cm^2	− 20	[68]
	6 mol/L KOH/2 mol/LKI/H_2O/PAM-CNF	110(− 40 °C)	− 63.3	− 40–20	Zn | air	743	2 mA/cm^2	− 40	[69]
	6 mol/L KOH/PAAm/G–CyBA/H_2O	252.2(− 50 °C) 431.7(100 °C)	*	− 50–100	Zn | air	620	5 mA/cm^2	− 50	[110]
	0.31 mmol/L SPDPA/0.31 mmol/L EA /0.31 mmol/L TFM/0.028 mmol/L AIBN/H_2O	3.26×10^{-3}(RT)	*	25–60	Na | $Na_3V_2(PO_4)_3$	93.4	270 mA/g	60	[111]
	1 mol/L LiTFSI/Li-IL/EMIM-TFSI/hBN/H_2O	> 1(RT)	*	RT–175	Li | Gr-LFP	150 160	0.1 C 4 C	RT 175	[112]
	LiTFSI/CMC/PAM/Acetamide/H_2O	12.8(30 °C)	71.7	− 20–20	$LiMn_2O_4$ | $Li_4Ti_5O_{12}$	40	1 C	− 20	[114]
	$Zn(CF_3SO_3)_2$/DMSO/PAAm/H_2O	*	*	− 40–60	Zn | $Zn_3V_2O_8$	175	2 A/g	− 40	[115]

Table 1 (continued)

Category	Electrolyte	Ionic conductivity (mS/cm)	Freezing point (°C)	Operating temperature range (°C)	Systems	Capacity (mAh/g)	Current density	T (°C)	References
	2 mol/L (Zn(OTf)$_2$/50% PEG/H$_2$O	0.37(− 20 °C)	− 93.04	− 20–80	Zn ∣ PANI@V$_2$O$_5$	82 310	0.2 A/g 50 mA/g	− 20 60	[116]
	2 mol/L ZnCl$_2$/3 mol/L NH$_4$Cl/10% H$_2$O/ PAMPS/PAAm	1.62(− 30 °C)	< − 50	− 30–80	Zn ∣ PANI	59.7 48.4	0.2 A/g 5 A/g	− 30 80	[117]
	3 mol/L Zn(OTf)$_2$/ H$_2$O/PAM	1.9(− 30 °C)	*	− 30–80	Zn ∣ Mg$_{1.5}$V$_2$O$_5$·H$_2$O	272 501	0.2 A/g	− 30 80	[126]
	6 mol/L KOH/0.2 mol/L Zn(Ac)$_2$/H$_2$O/PANa	5.7(− 20 °C) 16.3(50 °C)	< − 50	− 20–50	Zn ∣ NiCo@CC	108 137	490.2 mA/g 825.6 mA/g	− 20 50	[127]
	3 mol/L Zn(OTf)$_2$/ H$_2$O/glycerol/PVA	10.7(− 30 °C)	< − 30	− 30–60	Zn ∣ Mg$_{0.19}$V$_2$O$_5$·0.99H$_2$O	256.3 490.2	0.1 A/g	− 30 60	[60]
	2 mol/L ZnSO$_4$/0.2 mol/L MnSO$_4$/glycerol/cellulose/TEOS(CT3G30)	19.4(− 40 °C)	− 64.6	− 40–60	Zn ∣ MnO$_2$	211.9 277.3	0.2 A/g	− 40 20	[128]
	2 mol/L ZnSO$_4$/0.2 mol/L MnSO$_4$/H$_2$O/ elastomer-coated/EG-alginate /PAM	14.1(− 20 °C) 18.2(80 °C)	*	− 20–80	Zn ∣ MnO$_2$	165 105	0.2 A/g 2 A/g	− 20 80	[129]
	6 mol/L KOH/H$_2$O/G-CyBA /PAM/SP-DN	252.2(− 50 °C) 431.7(100 °C)	− 196	− 50–100	Zn ∣ air	620	5 mA/cm^2	− 50	[130]
	2 mol/L NaClO$_4$/ DMSO/H$_2$O	0.11(− 50 °C)	− 130	− 50–45	NaTi$_2$-(PO$_4$)$_3$@C ∣ AC	58	0.5 C	− 50	[25]
	LiTFSI/TMS/ Water(1:0.5:1)	1.03×10^{-4}(− 80 °C)	− 85	− 80–60	LiNi$_{0.5}$Mn$_{1.5}$O$_4$ ∣ Li$_4$Ti$_5$O$_{12}$	196.8	3 C	− 80	[31]
	LiTFSI/DOL/H$_2$O	*	− 95	− 50–RT	LiMn$_2$O$_4$ ∣ Li$_4$Ti$_5$O$_{12}$	86	0.1 C	− 50	[81]
	2 mol/L ZnSO$_4$/ 33.3% DMF/H$_2$O	1.27(70 °C) 0.04(− 30 °C)	− 32	− 30–70	Zn ∣ Ac	38.4 42	2 A/g 0.5 A/g	60 − 20	[82]
	2 mol/L ZnSO$_4$/ 40% EG/H$_2$O	6.9(− 40 °C)	*	− 40–20	Zn ∣ PANI–V$_2$O$_5$	130	0.2 A/g	− 20	[88]
	1 mol/L Li$_2$SO$_4$/ 40% EtG/H$_2$O	11.3(0 °C)	− 24.6	− 20–0	LiFePO$_4$	68	1 C	− 10	[83]
	2 mol/L ZnSO$_4$/0.2 mol/L MnSO$_4$/1% Et$_2$O/30% EG/H$_2$O	0.42(− 10 °C)	*	− 10–25	Zn ∣ CNT/MnO$_2$	65.1	3 A/g	− 10	[85]
	15.3 mol/L LiTFSI /50% AN/H$_2$O	0.63(− 20 °C)	48	− 20–60	LiMn$_2$O$_4$ ∣ Li$_4$Ti$_5$O$_{12}$	110	1 C	0	[86]
	12 mol/L SL/4 mol/L H$_2$O/3 mol/L LiClO$_4$	0.12(− 40 °C)	− 110	− 65–0	LiMn$_2$O$_4$ ∣ Li$_4$Ti$_5$O$_{12}$	93	25 mA/g	− 20	[94]
	1 mol/L Zn(TfO)$_2$/ 50% NMP/H$_2$O	1.9(− 20 °C)	*	− 20–20	Zn ∣ PANI	73	0.2 A/g	− 20	[95]
	1 mol/L Zn(OTf)$_2$/ DME/H$_2$O	1.06(− 40 °C)	− 52.4	− 40–25	Zn ∣ V$_2$O$_5$	212.4 499.8	0.5 A/g 0.2 A/g	− 40 RT	[96]
	3.5 mol/L Mg(ClO$_4$)$_2$ /1 mol/L Zn(ClO$_4$)$_2$/ H$_2$O	1.41(− 70 °C)	− 121	− 70 —25	Zn ∣ Pyrene-4,5,9,10-tetraone	101.5	0.5 C	− 70	[98]
	3.5 mol/L Mg(ClO$_4$)$_2$/ 0.5 mol/L NaClO$_4$/H$_2$O	4.86(− 60 °C)	< − 80	− 60–RT	AC ∣ NaTi$_2$(PO$_4$)$_3$@C	83.2	0.2 C	− 60	[99]

Table 1 (continued)

Category	Electrolyte	Ionic conductivity (mS/cm)	Freezing point (°C)	Operating temperature range (°C)	Systems	Capacity (mAh/g)	Current density	T (°C)	References
	3.86 mol/L CaCl$_2$/1 mol/L NaClO$_4$/H$_2$O	7.13(-50 °C)	< -50	-30–25	AC | Na$_2$CoFe(CN)$_6$	74.5	1 C	-30	[100]
	1 mol/L Zn(CF$_3$SO$_3$)$_2$ /50% DOL/H$_2$O	30(RT)	-51.2	-30–25	Zn | V$_2$O$_5$·1.6H$_2$O	131	0.1 A/g	-30	[101]
	0.8 mol/L Zn(OTf)$_2$/ PD/H$_2$O	*	*	25–100	Zn | Te-G-CNT	195.7	2 C	100	[109]
	0.5 mol/L ZnTFMS/ DMF/H$_2$O	18.9(25 °C)	-70.8	-70–150	Zn | PQ-MCT	31.3 196	0.2 A/g 2 A/g	-70 150	[133]
	1 mol/L Zn(OTf)$_2$/ DMAC/TMP/H$_2$O	*	*	-40–70	Zn | NaV$_3$O$_8$·1.5H$_2$O	85 120	0.1 A/g 5 A/g	-40 70	[119]
	4 mol/L Zn(BF$_4$)$_2$/EG/ H$_2$O	4.5(RT)	*	-30–40	Zn | V$_2$O$_5$	93	0.5 A/g	-15	[120]
	1 mol/L NaNO$_3$/Gly/ H$_2$O	8(RT)	< -80	-10–25	PTCDI | Ni$_2$ZnHCF	40	0.1 A/g	-10	[121]
	2 mol/L ZnSO$_4$ /50% EG/H$_2$O	*	-43.2	-40–80	Zn | PQ-MCT	20 152	0.2 A/g	-40 80	[123]
	2 mol/L ZnSO$_4$/50% MeOH/H$_2$O	16.8(25 °C)	-46	-20–60	Zn | PANI	186.3 249.7	0.1 A/g	-10 60	[124]
	1 mol/L Zn(OTf)$_2$ 72% AN/28% H$_2$O	28.6(-40 °C)	-55.3	-40–25	Zn | V$_2$O$_5$	114	0.05 A/g	-40	[125]
	7.6 mol/L ZnCl$_2$/0.05 mol/L SnCl$_2$/H$_2$O	0.8(-70 °C)	*	-70–20	Zn | VOPO$_4$	48.7 163	1/3 C	-70 20	[132]

materials [135–139]. Therefore, it is necessary to consider the effect of the cathode on the electrolyte in the design of a suitable electrolyte or when evaluating the performance of the cell at high temperatures.

Conclusions and Prospects

Compared with conventional commercial organic batteries, ARBs are cheap to produce, easy to assemble, intrinsically safe, and environmentally friendly. They, therefore, hold great promise for use in flexible and wearable electronics and as large-scale energy storage devices. However, the temperature of ARBs and the freezing or volatility of the electrolyte greatly affect their electrochemical performance, reliability, and safety, which limits their large-scale commercial application. Nevertheless, increasing numbers of studies are being conducted, and the development of ARBs is progressing.

This review systematically summarizes the challenges and solutions associated with the use of ARBs in different temperature regions, and the following three effective electrolyte improvement strategies are proposed: (1) increasing the solute concentration of the aqueous electrolyte, (2) introducing efficient additives to the electrolyte, and (3) utilizing a hydrogel electrolyte. Based on this review, the following main conclusions and suggestions are made:

1. The electrolyte is undoubtedly an important component of the battery. For non-room temperature use, it is recommended that electrolytes have high ionic conductivity, a low freezing point, low viscosity, a low free water content, and low flammability. In addition to ensuring that the electrolyte has these physical properties, it is necessary to conduct in-depth studies of the electrolyte structure to further understand its interfacial behavior at the electrode.

2. Hydrogel electrolytes engineered for wearable or portable devices require the aforementioned temperature adaptation and satisfactory electrochemical properties, but the mechanical properties in different environments also need to be ascertained.

3. In general, the sub-zero temperature performance of ARBs remains inferior to that of organic electrolytes because the freezing point of water is higher than that of most organic solvents. However, organic additives carry a certain degree of toxicity, and the addition of organic additives significantly reduces the ionic conductivity of the electrolyte. To maintain the competitiveness of ARBs, it is necessary to ensure their intrinsic safety and low cost,

and the continued exploration of high-safety and non-polluting organic/inorganic additives is still required.

4. It is also necessary to consider the compatibility of the electrolyte and electrode materials. Organic cathodes may dissolve in organic solvent-based electrolytes, while some inorganic cathodes may dissolve or decompose at high temperatures. An in-depth elucidation of the combination of electrolyte solvation structures and electrode reaction mechanisms is thus required, and advanced in situ or ex situ characterization at low and high temperatures is essential to obtain a deeper understanding of the electrochemical behavior.

5. To thoroughly explain the reaction mechanism at non-room temperature, it is also necessary to use advanced and temperature-adapted characterization techniques. Examples of current techniques include variable-temperature nuclear magnetic resonance, high-resolution neutron powder diffraction, in situ liquid/solid FTIR, in situ liquid/solid Raman spectroscopy, cryo-electron microscopy, and cryo-focused ion beam (cryo-FIB). However, quantifying each component and its precise distribution at a nanoscale resolution remains a rather challenging task, and more associated in-depth studies are required.

Declarations

**Conflict of interest** The authors declare that there is no conflict of interest.

References

1. Hou WH, Lu Y, Ou Y et al (2023) Recent advances in electrolytes for high-voltage cathodes of lithium-ion batteries. Trans Tianjin Univ 29(2):120–135

2. Wang L, Menakath A, Han F et al (2019) Identifying the components of the solid-electrolyte interphase in Li-ion batteries. Nat Chem 11(9):789–796

3. Armand M, Tarascon JM (2008) Building better batteries. Nature 451(7179):652–657

4. Dunn B, Kamath H, Tarascon JM (2011) Electrical energy storage for the grid: a battery of choices. Science 334(6058):928–935

5. Luo F, Feng X, Zeng L et al (2021) In situ simultaneous encapsulation of defective MoS_2 nanolayers and sulfur nanodots into SPAN fibers for high rate sodium-ion batteries. Chem Eng J 404:126430

6. Wang M, Meng Y, Li K et al (2022) Toward dendrite-free and anti-corrosion Zn anodes by regulating a bismuth-based energizer. eScience 2(5):509–517

7. Yao YX, Yao N, Zhou XR et al (2022) Ethylene-carbonate-free electrolytes for rechargeable Li-ion pouch cells at sub-freezing temperatures. Adv Mater 34(45):e2206448

8. Liu Z, Huang Y, Huang Y et al (2020) Voltage issue of aqueous rechargeable metal-ion batteries. Chem Soc Rev 49(1):180–232

9. Zhang X, Li J, Ao H et al (2020) Appropriately hydrophilic/hydrophobic cathode enables high-performance aqueous zinc-ion batteries. Energy Storage Mater 30:337–345

10. Zhang S, Li S, Lu Y (2021) Designing safer lithium-based batteries with nonflammable electrolytes: a review. eScience 1(2):163–177

11. Wang J, Wang B, Lu B (2020) Nature of novel 2D van der Waals heterostructures for superior potassium ion batteries. Adv Energy Mater 10(24):2000884

12. Huang Y, Li Z, Pei Z et al (2018) Solid-state rechargeable Zn/NiCo and Zn-air batteries with ultralong lifetime and high capacity: the role of a sodium polyacrylate hydrogel electrolyte. Adv Energy Mater 8(31):1802288

13. Wang H, Liu J, He J et al (2022) Pseudo-concentrated electrolytes for lithium metal batteries. eScience 2(5):557–565

14. Huang J, Guo Z, Ma Y et al (2019) Recent progress of rechargeable batteries using mild aqueous electrolytes. Small Meth 3(1):1800272

15. Wang D, Zhao Y, Liang G et al (2020) A zinc battery with ultra-flat discharge plateau through phase transition mechanism. Nano Energy 71:104583

16. Zhang Y, Zhao L, Liang Y et al (2022) Effect of electrolyte anions on the cycle life of a polymer electrode in aqueous batteries. eScience 2(1):110–115

17. Li H, Ma L, Han C et al (2019) Advanced rechargeable zinc-based batteries: recent progress and future perspectives. Nano Energy 62:550–587

18. Fang L, Cai Z, Ding Z et al (2019) Skin-inspired surface-microstructured tough hydrogel electrolytes for stretchable supercapacitors. ACS Appl Mater Interfaces 11(24):21895–21903

19. Ji X (2022) A perspective of $ZnCl_2$ electrolytes: the physical and electrochemical properties. eScience 1(2):99–107

20. Xu CX, Jiang J (2021) Electrolytes speed up development of zinc batteries. Rare Met 40(4):749–751

21. Jiang L, Lu Y, Zhao C et al (2019) Building aqueous K-ion batteries for energy storage. Nat Energy 4(6):495–503

22. Hubble D, Brown DE, Zhao Y et al (2022) Liquid electrolyte development for low-temperature lithium-ion batteries. Energy Environ Sci 15(2):550–578

23. Zhu K, Sun Z, Li Z et al (2023) Design strategies and recent advancements for low-temperature aqueous rechargeable energy storage. Adv Energy Mater 13(8):2203708

24. Zhang Q, Ma Y, Lu Y et al (2020) Modulating electrolyte structure for ultralow temperature aqueous zinc batteries. Nat Commun 11(1):4463

25. Nian Q, Wang J, Liu S et al (2019) Aqueous batteries operated at −50 ℃. Angew Chem Int Ed 58(47):16994–16999

26. Feng Y, Zhou L, Ma H et al (2022) Challenges and advances in wide-temperature rechargeable lithium batteries. Energy Environ Sci 15(5):1711–1759

27. Xu K (2004) Nonaqueous liquid electrolytes for lithium-based rechargeable batteries. Chem Rev 104(10):4303–4417

28. Hou J, Yang M, Wang D et al (2020) Lithium-ion batteries: fundamentals and challenges of lithium ion batteries at temperatures between −40 and 60 ℃. Adv Energy Mater 10(18):2070079

29. Dong X, Wang YG, Xia Y (2021) Promoting rechargeable batteries operated at low temperature. Acc Chem Res 54(20):3883–3894

30. Wang M, Li T, Yin Y et al (2022) A −60 ℃ low-temperature aqueous lithium ion-bromine battery with high power density enabled by electrolyte design. Adv Energy Mater 12(25):2200728

31. Shang Y, Chen S, Chen N et al (2022) A universal strategy for high-voltage aqueous batteries via lone pair electrons as the hydrogen bond-breaker. Energy Environ Sci 15(6):2653–2663

32. Zhang X, Chen J, Xu Z et al (2022) Aqueous electrolyte with moderate concentration enables high-energy aqueous rechargeable lithium ion battery for large scale energy storage. Energy Storage Mater 46:147–154

33. Lu C, Chen X (2020) All-temperature flexible supercapacitors enabled by antifreezing and thermally stable hydrogel electrolyte. Nano Lett 20(3):1907–1914

34. Wang H, Chen Z, Ji Z et al (2021) Temperature adaptability issue of aqueous rechargeable batteries. Mater Today Energy 19:100577

35. Li F, Hu X (2021) Zinc metal energy storage devices under extreme conditions of low temperatures. Batter Supercaps 4(3):389–406

36. Ramanujapuram A, Yushin G (2018) Understanding the exceptional performance of lithium-ion battery cathodes in aqueous electrolytes at subzero temperatures. Adv Energy Mater 8(35):1802624

37. Liu Z, Luo X, Qin L et al (2022) Progress and prospect of low-temperature zinc metal batteries. Adv Powder Mater 1(2):100011

38. Tamtögl A, Bahn E, Sacchi M et al (2021) Motion of water monomers reveals a kinetic barrier to ice nucleation on graphene. Nat Commun 12(1):3120

39. Deng T, Zhang W, Zhang H et al (2018) Anti-freezing aqueous electrolyte for high-performance $Co(OH)_2$ supercapacitors at −30 ℃. Energy Technol 6(4):605–612

40. Ma L, Li N, Long C et al (2019) Achieving both high voltage and high capacity in aqueous zinc-ion battery for record high energy density. Adv Funct Mater 29(46):1906142

41. Zhang H, Liu X, Li H et al (2020) High-voltage operation of a V_2O_5 cathode in a concentrated gel polymer electrolyte for high-energy aqueous zinc batteries. ACS Appl Mater Interfaces 12(13):15305–15312

42. Lukatskaya MR, Feldblyum JI, Mackanic DG et al (2018) Concentrated mixed cation acetate "water-in-salt" solutions as green and low-cost high voltage electrolytes for aqueous batteries. Energy Environ Sci 11(10):2876–2883

43. Zhang Q, Xia K, Ma Y et al (2021) Chaotropic anion and fast-kinetics cathode enabling low-temperature aqueous Zn batteries. ACS Energy Lett 6(8):2704–2712

44. Liang G, Gan Z, Wang X et al (2021) Reconstructing vanadium oxide with anisotropic pathways for a durable and fast aqueous K-ion battery. ACS Nano 15(11):17717–17728

45. Jiang L, Liu L, Yue J et al (2020) High-voltage aqueous Na-ion battery enabled by inert-cation-assisted water-in-salt electrolyte. Adv Mater 32(2):e1904427

46. Yue J, Lin L, Jiang L et al (2020) Interface concentrated-confinement suppressing cathode dissolution in water-in-salt electrolyte. Adv Energy Mater 10(36):2000665

47. Becker M, Kühnel RS, Battaglia C (2019) Water-in-salt electrolytes for aqueous lithium-ion batteries with liquidus temperatures below −10 ℃. Chem Commun 55(80):12032–12035

48. Reber D, Kühnel RS, Battaglia C (2019) Suppressing crystallization of water-in-salt electrolytes by asymmetric anions enables low-temperature operation of high-voltage aqueous batteries. ACS Mater Lett 1(1):44–51

49. Sun T, Yuan X, Wang K et al (2021) An ultralow-temperature aqueous zinc-ion battery. J Mater Chem A 9(11):7042–7047

50. Borodin O, Self J, Persson KA et al (2020) Uncharted waters: super-concentrated electrolytes. Joule 4(1):69–100

51. Yamada Y (2020) Concentrated battery electrolytes: developing new functions by manipulating the coordination states. Bull Chem Soc Jpn 93(1):109–118

52. Song M, Tan H, Chao D et al (2018) Recent advances in Zn-ion batteries. Adv Funct Mater 28(41):1802564

53. Yamada Y, Yaegashi M, Abe T et al (2013) A superconcentrated ether electrolyte for fast-charging Li-ion batteries. Chem Commun 49(95):11194–11196

54. Zhang H, Liu X, Li H et al (2021) Challenges and strategies for high-energy aqueous electrolyte rechargeable batteries. Angew Chem Int Ed 60(2):598–616

55. Chao D, Qiao SZ (2020) Toward high-voltage aqueous batteries: super- or low-concentrated electrolyte? Joule 4(9):1846–1851

56. Yu M, Lu Y, Zheng H et al (2018) New insights into the operating voltage of aqueous supercapacitors. Chem-Eur J 24(15):3639–3649

57. Sui X, Guo H, Chen P et al (2019) Zwitterionic osmolyte-based hydrogels with antifreezing property, high conductivity, and stable flexibility at subzero temperature. Adv Funct Mater 30(7):1907986

58. Wang M, Wang Q, Ding X et al (2022) The prospect and challenges of sodium-ion batteries for low-temperature conditions. Interdiscipl Mater 1(3):373–395

59. Huang J, Dong X, Wang N et al (2022) Building low-temperature batteries: non-aqueous or aqueous electrolyte? Curr Opin Electrochem 33:100949

60. Zhou W, Chen J, Chen M et al (2020) An environmentally adaptive quasi-solid-state zinc-ion battery based on magnesium vanadate hydrate with commercial-level mass loading and anti-freezing gel electrolyte. J Mater Chem A 8(17):8397–8409

61. Shi Y, Wang R, Bi S et al (2023) An anti-freezing hydrogel electrolyte for flexible zinc-ion batteries operating at −70 ℃. Adv Funct Mater 33(24):2214546

62. Hu Y, Shi R, Ren Y et al (2022) A "two-in-one" strategy for flexible aqueous batteries operated at −80 ℃. Adv Funct Mater 32(27):2203081

63. Liu T, Liu KT, Wang J et al (2021) Achievement of a polymer-free KAc gel electrolyte for advanced aqueous K-ion battery. Energy Storage Mater 41:133–140

64. Mo F, Li Q, Liang G et al (2021) A self-healing crease-free supramolecular all-polymer supercapacitor. Adv Sci 8(12):2100072

65. Fu Q, Hao S, Meng L et al (2021) Engineering self-adhesive polyzwitterionic hydrogel electrolytes for flexible zinc-ion hybrid capacitors with superior low-temperature adaptability. ACS Nano 15(11):18469–18482

66. Fu Q, Hao S, Zhang X et al (2023) All-round supramolecular zwitterionic hydrogel electrolytes enabling environmentally adaptive dendrite-free aqueous zinc ion capacitors. Energy Environ Sci 16(3):1291–1311

67. Gong JP, Katsuyama Y, Kurokawa T et al (2003) Double-network hydrogels with extremely high mechanical strength. Adv Mater 15(14):1155–1158

68. Sun N, Lu F, Yu Y et al (2020) Alkaline double-network hydrogels with high conductivities, superior mechanical performances, and antifreezing properties for solid-state zinc-air batteries. ACS Appl Mater Interfaces 12(10):11778–11788

69. Zhang Y, Qin H, Alfred M et al (2021) Reaction modifier system enable double-network hydrogel electrolyte for flexible zinc-air batteries with tolerance to extreme cold conditions. Energy Storage Mater 42:88–96

70. Zhao Y, Chen Z, Mo F et al (2020) Aqueous rechargeable metal-ion batteries working at subzero temperatures. Adv Sci 8(1):2002590

71. Zhou D, Chen F, Handschuh-Wang S et al (2019) Biomimetic extreme-temperature- and environment-adaptable hydrogels. ChemPhysChem 20(17):2139–2154

72. Zheng J, Engelhard MH, Mei D et al (2017) Electrolyte additive enabled fast charging and stable cycling lithium metal batteries. Nat Energy 2:17012

73. Song M, Zhong CL (2022) Achieving both high reversible and stable Zn anode by a practical glucose electrolyte additive toward high-performance Zn-ion batteries. Rare Met 41(2):356–360

74. Ren HT, Zhang ZQ, Zhang JZ et al (2022) Improvement of stability and solid-state battery performances of annealed 70Li$_2$S–30P$_2$S$_5$ electrolytes by additives. Rare Met 41:106–114

75. Tang X, Zhang WC, Cao LY (2022) Multifunctional high-fluorine-content molecule with high dipole moment as electrolyte additive for high performance lithium metal batteries. Rare Met 41(3):726–729

76. Jin Y, Han KS, Shao Y et al (2020) Stabilizing zinc anode reactions by polyethylene oxide polymer in mild aqueous electrolytes. Adv Funct Mater 30(43):2003932

77. Han W, Ardhi R, Liu GC (2022) Dual impact of superior SEI and separator wettability to inhibit lithium dendrite growth. Rare Met 41(2):353–355

78. Guo Y, Liu J, Yang Q et al (2020) Metal-tuned acetylene linkages in hydrogen substituted graphdiyne boosting the electrochemical oxygen reduction. Small 16(10):e1907341

79. Xu Z, Yang J, Li H et al (2019) Electrolytes for advanced lithium ion batteries using silicon-based anodes. J Mater Chem A 7(16):9432–9446

80. Sun P, Ma L, Zhou W et al (2021) Simultaneous regulation on solvation shell and electrode interface for dendrite-free Zn ion batteries achieved by a low-cost glucose additive. Angew Chem Int Ed 60(33):18247–18255

81. Ma Z, Chen J, Vatamanu J et al (2022) Expanding the low-temperature and high-voltage limits of aqueous lithium-ion battery. Energy Storage Mater 45:903–910

82. Xiong P, Kang Y, Yao N et al (2023) Zn-ion transporting, in situ formed robust solid electrolyte interphase for stable zinc metal anodes over a wide temperature range. ACS Energy Lett 8(3):1613–1625

83. Tron A, Jeong S, Park YD et al (2019) Aqueous lithium-ion battery of nano-LiFePO$_4$ with antifreezing agent of ethyleneglycol for low-temperature operation. ACS Sustain Chem Eng 7(17):14531–14538

84. Lin C, Yang X, Xiong P et al (2022) High-rate, large capacity, and long life dendrite-free Zn metal anode enabled by trifunctional electrolyte additive with a wide temperature range. Adv Sci 9(21):e2201433

85. Wang A, Zhou W, Huang A et al (2021) Developing improved electrolytes for aqueous zinc-ion batteries to achieve excellent cyclability and antifreezing ability. J Colloid Interface Sci 586:362–370

86. Chen J, Vatamanu J, Xing L et al (2020) Improving electrochemical stability and low-temperature performance with water/acetonitrile hybrid electrolytes. Adv Energy Mater 10(3):1902654

87. Ma Q, Gao R, Liu Y et al (2022) Regulation of outer solvation shell toward superior low-temperature aqueous zinc-ion batteries. Adv Mater 34(49):e2207344

88. Chang N, Li T, Li R et al (2020) An aqueous hybrid electrolyte for low-temperature zinc-based energy storage devices. Energy Environ Sci 13(10):3527–3535

89. Cai S, Chu X, Liu C et al (2021) Water-salt oligomers enable supersoluble electrolytes for high-performance aqueous batteries. Adv Mater 33(13):e2007470

90. Yang Y, Yang Y, Cao Y et al (2021) Anti-freezing, resilient and tough hydrogels for sensitive and large-range strain and pressure sensors. Chem Eng J 403:126431

91. Ding Y, Zhong X, Yuan C et al (2021) Sodium alginate binders for bivalency aqueous batteries. ACS Appl Mater Interfaces 13(17):20681–20688

92. Ahn SM, Suk J, Kim DY et al (2017) High-performance lithium-oxygen battery electrolyte derived from optimum combination of solvent and lithium salt. Adv Sci 4(10):1700235

93. Rong JZ, Cai TX, Bai YZ et al (2022) A free-sealed high-voltage aqueous polymeric sodium battery enabling operation at −25 ℃. Cell Rep Phys Sci 3(3):100805

94. Liu J, Yang C, Chi X et al (2022) Water/sulfolane hybrid electrolyte achieves ultralow-temperature operation for high-voltage aqueous lithium-ion batteries. Adv Funct Mater 32(1):2106811

95. Zhao Z, Yin J, Yin J et al (2023) End-capping of hydrogen bonds: a strategy for blocking the proton conduction pathway in aqueous electrolytes. Energy Storage Mater 55:479–489

96. Dong Y, Zhang N, Wang Z et al (2023) Cell-nucleus structured electrolyte for low-temperature aqueous zinc batteries. J Energy Chem 83:324–332

97. Yao N, Chen X, Fu ZH et al (2022) Applying classical, *ab initio*, and machine-learning molecular dynamics simulations to the liquid electrolyte for rechargeable batteries. Chem Rev 122(12):10970–11021

98. Sun T, Zheng S, Du H et al (2021) Synergistic effect of cation and anion for low-temperature aqueous zinc-ion battery. Nanomicro Lett 13(1):204

99. Zhu K, Sun Z, Jin T et al (2022) Tailoring pure inorganic electrolyte for aqueous sodium-ion batteries operating at –60 ℃. Batter Supercaps 5(12):e202200308

100. Zhu K, Li Z, Sun Z et al (2022) Inorganic electrolyte for low-temperature aqueous sodium ion batteries. Small 18(14):e2107662

101. Du H, Wang K, Sun T et al (2022) Improving zinc anode reversibility by hydrogen bond in hybrid aqueous electrolyte. Chem Eng J 427:131705

102. Liu S, Mao J, Pang WK et al (2021) Tuning the electrolyte solvation structure to suppress cathode dissolution, water reactivity, and Zn dendrite growth in zinc-ion batteries. Adv Funct Mater 31(38):2104281

103. Ahmed F, Rahman MM, Chandra Sutradhar S et al (2019) Novel divalent organo-lithium salts with high electrochemical and thermal stability for aqueous rechargeable Li-Ion batteries. Electrochim Acta 298:709–716

104. Jin D, Choi S, Jang W et al (2019) Bismuth islands for low-temperature sodium-beta alumina batteries. ACS Appl Mater Interfaces 11(3):2917–2924

105. Sui Y, Ji X (2021) Anticatalytic strategies to suppress water electrolysis in aqueous batteries. Chem Rev 121(11):6654–6695

106. Zhang Y, Xu J, Li Z et al (2022) All-climate aqueous Na-ion batteries using water-in-salt electrolyte. Sci Bull 67(2):161–170

107. Yan L, Qi YE, Dong X et al (2021) Ammonium-ion batteries with a wide operating temperature window from −40 to 80℃. eScience 1(2):212–218

108. Xie J, Liang Z, Lu YC (2020) Molecular crowding electrolytes for high-voltage aqueous batteries. Nat Mater 19(9):1006–1011

109. Wang J, Yang Y, Wang Y et al (2022) Working aqueous Zn metal batteries at 100 ℃. ACS Nano 16(10):15770–15778

110. Gu C, Xie XQ, Liang Y et al (2021) Small molecule-based supramolecular-polymer double-network hydrogel electrolytes for ultra-stretchable and waterproof Zn-air batteries working from −50 to 100 ℃. Energy Environ Sci 14(8):4451–4462

111. Zheng J, Yang Y, Li W et al (2020) Novel flame retardant rigid spirocyclic biphosphate based copolymer gel electrolytes for sodium ion batteries with excellent high-temperature performance. J Mater Chem A 8(43):22962–22968

112. Hyun WJ, de Moraes ACM, Lim JM et al (2019) High-modulus hexagonal boron nitride nanoplatelet gel electrolytes for solid-state rechargeable lithium-ion batteries. ACS Nano 13(8):9664–9672

113. Jiang Y, Ma K, Sun M et al (2023) All-climate stretchable dendrite-free Zn-ion hybrid supercapacitors enabled by hydrogel electrolyte engineering. Energy Environ Mater 6(2):e12357

114. Hou X, Pollard TP, He X et al (2022) "Water-in-eutectogel" electrolytes for quasi-solid-state aqueous lithium-ion batteries. Adv Energy Mater 12(23):2200401

115. Lu H, Hu J, Wang L et al (2022) Multi-component crosslinked hydrogel electrolyte toward dendrite-free aqueous Zn ion batteries with high temperature adaptability. Adv Funct Mater 32(19):2112540

116. Zhou J, Yuan H, Li J et al (2022) Highly reversible and stable Zn metal anode under wide temperature conditions enabled by modulating electrolyte chemistry. Chem Eng J 442:136218

117. Li X, Wang H, Sun X et al (2021) Flexible wide-temperature zinc-ion battery enabled by an ethylene glycol-based organohydrogel electrolyte. ACS Appl Energy Mater 4(11):12718–12727

118. Zhao M, Lv Y, Zhao S et al (2022) Simultaneously stabilizing both electrodes and electrolytes by a self-separating organometallics interface for high-performance zinc-ion batteries at wide temperatures. Adv Mater 34(49):e2206239

119. Wang Y, Wang Z, Pang WK et al (2023) Solvent control of water O–H bonds for highly reversible zinc ion batteries. Nat Commun 14(1):2720

120. Han D, Cui C, Zhang K et al (2022) A non-flammable hydrous organic electrolyte for sustainable zinc batteries. Nat Sustain 5(3):205–213

121. Sun Y, Zhang Y, Xu Z et al (2022) Dilute hybrid electrolyte for low-temperature aqueous sodium-ion batteries. Chemsuschem 15(23):e202201362

122. Sun T, Nian Q, Du H et al (2022) Aqueous proton battery stably operates in mild electrolyte and low-temperature conditions. J Mater Chem A 10(33):17288–17296

123. Wang N, Yang Y, Qiu X et al (2020) Stabilized rechargeable aqueous zinc batteries using ethylene glycol as water blocker. Chemsuschem 13(20):5556–5564

124. Hao J, Yuan L, Ye C et al (2021) Boosting zinc electrode reversibility in aqueous electrolytes by using low-cost antisolvents. Angew Chem Int Ed 60(13):7366–7375

125. Wang J, Zhu Q, Li F et al (2022) Low-temperature and high-rate Zn metal batteries enabled by mitigating Zn^{2+} concentration polarization. Chem Eng J 433:134589

126. Deng W, Zhou Z, Li Y et al (2020) High-capacity layered magnesium vanadate with concentrated gel electrolyte toward high-performance and wide-temperature zinc-ion battery. ACS Nano 14(11):15776–15785

127. Wang H, Liu J, Wang J et al (2019) Concentrated hydrogel electrolyte-enabled aqueous rechargeable NiCo// Zn battery working from –20 to 50 ℃. ACS Appl Mater Interfaces 11(1):49–55

128. Chen M, Chen J, Zhou W et al (2021) Realizing an all-round hydrogel electrolyte toward environmentally adaptive dendrite-free aqueous Zn–MnO₂ batteries. Adv Mater 33(9):e2007559

129. Mo F, Liang G, Wang D et al (2019) Biomimetic organohydrogel electrolytes for high-environmental adaptive energy storage devices. EcoMat 1(1):e12008

130. Gu C, Xie XQ, Liang Y et al (2021) Small molecule-based supramolecular-polymer double-network hydrogel electrolytes for ultra-stretchable and waterproof Zn-air batteries working from −50 to 100 ℃. Energy Environ Sci 14(8):4451–4462

131. Yesibolati N, Umirov N, Koishybay A et al (2015) High performance Zn/LiFePO₄ aqueous rechargeable battery for large scale applications. Electrochim Acta 152:505–511

132. Cao L, Li D, Soto FA et al (2021) Highly reversible aqueous zinc batteries enabled by zincophilic-zincophobic interfacial layers and interrupted hydrogen-bond electrolytes. Angew Chem Int Ed 60(34):18845–18851

133. Wang N, Dong X, Wang B et al (2020) Zinc-organic battery with a wide operation-temperature window from –70 to 150 ℃. Angew Chem Int Ed 59(34):14577–14583

134. Liu K, Liu Y, Lin D et al (2018) Materials for lithium-ion battery safety. Sci Adv 4(6):eaas9820

135. Yuan Z, Xiao F, Fang Y et al (2023) Defect engineering on VO₂(B) nanoleaves/graphene oxide for the high performance of cathodes of zinc-ion batteries with a wide temperature range. J Power Sources 559:232688

136. Yuan Z, Yang X, Lin C et al (2023) Progressive activation of porous vanadium nitride microspheres with intercalation-conversion reactions toward high performance over a wide temperature range for zinc-ion batteries. J Colloid Interface Sci 640:487–497

137. Wang Y, Xiao F, Chen X et al (2023) Extraordinarily stable and wide-temperature range sodium/potassium-ion batteries based on 1D SnSe₂-SePAN composite nanofibers. InfoMat 5(10):e12467

138. Xiong P, Zhang Y, Zhang J et al (2022) Recent progress of artificial interfacial layers in aqueous Zn metal batteries. EnergyChem 4(4):100076

139. Lei Z, Zheng J, He X et al (2023) Defect-rich WS₂–SPAN nanofibers for sodium/potassium-ion batteries: ultralong lifespans and wide-temperature workability. Inorg Chem Front 10(4):1187–1196
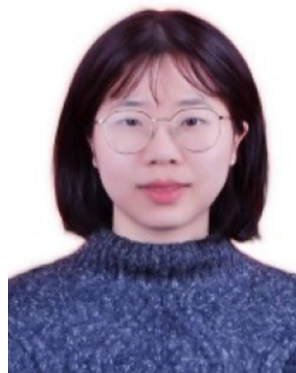
Lingjun He is currently pursuing a Master's degree with Professor Lingxing Zeng in the School of Chemistry and Materials at Fujian Normal University. She received her BSc degree from the School of Materials Science and Engineering, Qingdao University, in 2020. Her current research focuses on the engineering of interfacial modification of aqueous zinc-ion batteries.

Chuyuan Lin is currently doing her PhD research under Professor Lingxing Zeng at the School of Environment and Resources, Fujian Normal University. She received her BSc degree from the School of Chemical and Materials Engineering, Huizhou University, in 2020. Her current research focuses on the modification of electrolytes for zinc-ion batteries.

Peixun Xiong is currently working with Professor Stefan Kaskel as a Humboldt Research Fellow at School of Inorganic Chemistry I, Technische Universität Dresden. Previously, he worked with Professor Ho Seok Park as a postdoctoral researcher at Sungkyunkwan University. He received his PhD in 2020 from the School of Materials Science and Engineering, Tianjin University, MS in 2016, and BS in 2013 from the College of Chemistry, Fuzhou University. He has published more than 70 papers in Frontiers journals. His current research mainly focuses on the design of electrode/electrolyte interphase for electrochemical energy storage devices.

Fuyu Xiao is currently doing her PhD research under Professor Qinghua Chen at the School of Environment and Resources, Fujian Normal University. She received her BSc degree from the College of Chemistry, Fuzhou University. Her current research focuses on designing the electrodes and electrolytes for zinc-ion batteries.

Qingrong Qian is the dean of the College of Environment and Resources of Fujian Normal University. He has presided over or participated in more than 20 projects, including the National Key Research and Development Program of China and National Natural Science Foundation of China, and has published more than 200 academic papers. He has received 4 second-class awards and 2 third-class awards for scientific and technological progress in Fujian Province. He is mainly engaged in the research of solid waste resource recycling and high-quality utilization, etc.

Qinghua Chen is vice president of Fujian Normal University, director of the Engineering Research Center of Polymer Green Recycling of Ministry of Education, a national candidate of the Hundred Million Talents Project and an outstanding talent of the Ministry of Education in the New Century. He is the chief scientist of National Key Research and Development Program of China. He has won 20 Provincial and Ministerial Science and Technology Progress Awards and published more than 300 academic papers. He is mainly engaged in the research of environment-friendly materials and comprehensive utilization of solid waste.

Lingxing Zeng is a professor at the College of Environment and Resources of Fujian Normal University, deputy director of the Fujian Provincial Key Laboratory, and Young Top Talent of Fujian Province. He hosted two State Research Projects including National Key Research and Development Program of China and National Natural Science Foundation of China. He has published more than 100 papers in Frontiers journals. In recent years, he is engaged in research on electrochemical energy storage materials and devices and recycling of spent batteries.